Glycoproteomics Reveals Decorin Peptides With Anti-Myostatin Activity in Human Atrial Fibrillation

BACKGROUND: Myocardial fibrosis is a feature of many cardiac diseases. We used proteomics to profile glycoproteins in the human cardiac extracellular matrix (ECM).

METHODS: Atrial specimens were analyzed by mass spectrometry after extraction of ECM proteins and enrichment for glycoproteins or glycopeptides.

RESULTS: ECM-related glycoproteins were identified in left and right atrial appendages from the same patients. Several known glycosylation sites were confirmed. In addition, putative and novel glycosylation sites were detected. On enrichment for glycoproteins, peptides of the small leucine-rich proteoglycan decorin were identified consistently in the flowthrough. Of all ECM proteins identified, decorin was found to be the most fragmented. Within its protein core, 18 different cleavage sites were identified. In contrast, less cleavage was observed for biglycan, the most closely related proteoglycan. Decorin processing differed between human ventricles and atria and was altered in disease. The C-terminus of decorin, important for the interaction with connective tissue growth factor, was detected predominantly in ventricles in comparison with atria. In contrast, atrial appendages from patients in persistent atrial fibrillation had greater levels of full-length decorin but also harbored a cleavage site that was not found in atrial appendages from patients in sinus rhythm. This cleavage site preceded the N-terminal domain of decorin that controls muscle growth by altering the binding capacity for myostatin. Myostatin expression was decreased in atrial appendages of patients with persistent atrial fibrillation and hearts of decorin null mice. A synthetic peptide corresponding to this decorin region dose-dependently inhibited the response to myostatin in cardiomyocytes and in perfused mouse hearts.

CONCLUSIONS: This proteomics study is the first to analyze the human cardiac ECM. Novel processed forms of decorin protein core, uncovered in human atrial appendages, can regulate the local bioavailability of antihypertrophic and profibrotic growth factors.

Javier Barallobre-Barreiro, PhD
Shashi K. Gupta, PhD
Anna Zoccarato, PhD
Rika Kitazume-Taneike, MD
Marika Fava, MSc
Xiaoke Yin, PhD
Tessa Werner, MSc
Marc N. Hirt, MD, PhD
Anna Zampetaki, PhD
Alessandro Viviano, MD
Mei Chong, PhD
Marshall Bern, PhD
Antonios Kourliouros, MD
Nieves Domenech, PhD
Peter Willeit, MD, PhD
Ajay M. Shah, MD
Marjan Jahangiri, MD
Liliana Schaefer, MD
Jens W. Fischer, PhD
Renato V. Iozzo, MD
Rosa Viner, PhD
Thomas Thum, MD, PhD
Joerg Heineke, MD
Antoine Kichler, PhD
Kinya Otsu, MD, PhD
Manuel Mayr, MD, PhD

Correspondence to: Manuel Mayr, MD, PhD, King's British Heart Foundation Centre, King's College London, 125 Coldharbour Ln, London, SE5 9NU, United Kingdom. E-mail manuel.mayr@kcl.ac.uk

Sources of Funding, see page 830

Key Words: atrial fibrillation ■ cardiovascular diseases ■ extracellular matrix ■ mass spectrometry ■ proteomics

CLINICAL PERSPECTIVE

What Is New?

- We used proteomics to analyze the extracellular matrix in human atrial appendages. By using novel mass spectrometry methods, we provide the first comprehensive characterization of human cardiac extracellular matrix proteins, including the identification of glycosylation sites.
- We found that decorin, a small and leucine-rich proteoglycan, is truncated in atria in comparison with ventricles, resulting in the loss of the binding site for connective tissue growth factor. In atrial fibrillation, decorin is increased but an additional cleavage site gives rise to peptides with myostatin-binding properties. These decorin peptides antagonize myostatin.

What Are the Clinical Implications?

- Atrial fibrillation is the most common arrhythmia encountered in clinical practice, and myostatin inhibition has been implicated as a substrate for atrial fibrillation. Myostatin expression was reduced in patients with atrial fibrillation and in hearts from decorin null mice.
- Peptides generated from the cleavage of extracellular matrix proteins such as decorin constitute a local regulatory mechanism for the bioactivity and bioavailability of growth factors in human cardiac tissue.

The importance of the extracellular matrix (ECM) is being recognized increasingly, gradually overturning the concept that the cardiac ECM is inert. ECM proteins not only account for physiological properties of the cardiac tissue, but also contribute to fibrosis and hypertrophy in disease. Fibrosis not only involves structural proteins, but also matricellular proteins, predominantly glycoproteins. Because of the continuous need for dynamic adaptation in the heart, matricellular proteins are of particular importance. Previous studies have demonstrated that ECM deposition facilitates the development of ectopic pacemakers and late potentials as a result of inhomogeneous stimulus conduction, and also can lead to fluctuations in membrane potential.[1] Thus, atrial fibrotic remodeling has been implicated as a potential therapeutic target in atrial fibrillation (AF).[2]

Proteomics offers the ability to quantify multiple proteins simultaneously without the constraints of antibodies. Most proteomics studies, including the ones on AF, have investigated the cellular proteome.[3,4] We previously have developed a sequential extraction procedure to reduce cellular proteins before studying ECM remodeling in a porcine model of ischemia/reperfusion injury.[5] No proteomics study has been conducted on the human cardiac ECM.

Therefore, the aims of the present study were 4-fold: (1) to provide a comprehensive characterization of ECM proteins in human atrial appendages, (2) to interrogate protein glycosylation of matricellular proteins, (3) to explore regional differences in the cardiac ECM composition, and (4) to interrogate ECM remodeling in the context of AF. We discovered extensive cleavage in the protein core of the proteoglycan decorin, a key constituent of the cardiac microenvironment. Decorin is a member of the small leucine-rich proteoglycan (SLRP) family[6,7] and regulates collagen fibrillogenesis, and a variety of other ECM molecules involved in cell signaling, as well.[8] Processed forms of decorin detected in the human cardiac ECM had myostatin and connective tissue growth factor (CTGF) binding properties that might contribute to the pathophysiology of AF by regulating the bioavailability of growth factors.

METHODS

An expanded Methods section is available in the online-only Data Supplement. UK, REC number [06/Q0803/69] corresponding to EudraCT number: 2006-005272-40). Atrial tissue was obtained from the atrial appendages during cardiopulmonary bypass and just after cardioplegic arrest of the heart.[4]

ECM Extraction

ECM protein enrichment was performed using our previously published 3-step extraction method, involving sequential incubation with 0.5 mol/L NaCl for 1 hour, 0.1% sodium dodecyl sulfate for 16 hours, and a final incubation for 72 hours with 4 mol/L guanidine hydrochloride.[5] Matched samples from both atria (n=5) were enriched further in ECM glycoproteins using a lectin binding–based protocol (ie, wheat germ agglutinin and concanavalin A). Guanidine hydrochloride extracts (input), glycoprotein-enriched extracts, and the flowthrough were enzymatically deglycosylated. Gel electrophoresis for deglycosylated proteins was performed using 4% to 12% Bis-Tris gradient gels. Gels were fixed and silver stained. The entire gel lanes were excised and digested using trypsin.[5] For direct glycopeptide identification, proteins were digested in solution without deglycosylation.

Mass Spectrometry Analyses

Liquid chromatography tandem mass spectrometry (MS/MS) acquisition was performed as previously described.[9] MS/MS peak lists were matched to a human database using Mascot (version 2.3.01, Matrix Science). Two missed trypsin cleavages were allowed. An additional, no-enzyme search was performed to identify peptides derived from nontryptic cleavages. For the identification of the glycosylation sites, a direct glycopeptide strategy was pursued using a combination of different fragmentation modes on an Orbitrap Elite MS as published elsewhere.[10]

Circulation. 2016;134:817–832. DOI: 10.1161/CIRCULATIONAHA.115.016423

P(CAGA)12-Luciferase Reporter Assay

HEK293 cells (ATCC) were transfected with the pGL3(CAGA)12-luciferase reporter plasmid. Recombinant mouse myostatin was added at a final concentration of 2.5 nmol/L ± decorin N-terminal peptides at different concentrations.[11] The HEK293 cells were cultured for 24 hours and were then lysed and luciferase activity was assayed.

Proton Nuclear Magnetic Resonance Spectroscopy

Metabolites from mouse cardiac tissue were extracted using a methanol-based procedure. Nuclear magnetic resonance (NMR) spectra were acquired on a 700-MHz Bruker spectrometer by using 9.3 kHz spectral width and 32 000 data points with acquisition time of 1.67 s, relaxation delay of 5 s, and 128 scans. The resulting spectra were processed to 65 536 data points and corrected for phasing and zero referencing by using NMRLab software.

Functional Experiments

To test the biological effects of decorin peptides, neonatal rat cardiomyocytes were used for in vitro experiments, and hearts from 10- to 12-week-old C57BL/6J male mice were perfused in a Langendorff system. Details are given in the online-only Data Supplement.

Statistical Analysis

Clinical characteristics are summarized as mean± standard deviation or as percentages, and tested for differences across groups using unpaired *t* tests for unequal variances or Fisher exact tests. For all significance testing, a 2-tailed $P<0.05$ was deemed significant.

RESULTS

Glycoproteomic Characterization of the ECM in Human Atria

Atrial appendages were obtained from patients undergoing coronary artery bypass grafting. The clinical characteristics and average atrial sizes of the patient cohort (n=14) are summarized in Table I in the online-only Data Supplement. ECM protein extracts were prepared as described previously[5] and analyzed by using a high mass accuracy tandem mass spectrometer (Figure 1A). All identified extracellular proteins are listed in Table II in the online-only Data Supplement.

We also obtained left and right atrial appendages (LAA and RAA) from the same patients undergoing cardiac surgery (n=5 each) and added enrichment steps for glycoproteins (Figure 1A). Peptides belonging to glycoproteins doubled on enrichment for glycoproteins (Figure I in the online-only Data Supplement). The identified ECM-related glycoproteins, and their distribution, as well, in the input (guanidine hydrochloride extracts), glycoprotein-enriched fraction, and unbound flowthrough are shown in Table III and Figure II in the online-only Data Supplement, respectively. In the glycoprotein-enriched fraction, levels of nidogen 2, cadherin 2 and basal cell adhesion molecule were more abundant in LAA, whereas latent transforming growth factor-β–binding protein 4, fibulin 2, lumican, and vitronectin were increased in RAA (Figure 1B). The latter findings were validated by immunoblotting of the original input material (Figure 1C and 1D).

Next, we combined a direct MS/MS method with glycoprotein or glycopeptide enrichment strategies for the identification of the glycosylation sites (Figure 1A). In total, 65 *N*- and *O*-linked glycosylation sites were identified in 35 extracellular proteins. Several known glycosylation sites were confirmed. In addition, putative and novel glycosylation sites were detected (Table IV in the online-only Data Supplement). Identified *N*-glycoforms were mostly complex, some sialylated or core fucosylated. Minor presences of high mannose and hybrid glycans were observed. *O*-Linked glycans were predominantly core 1 or 2 types with or without sialic acid. A summary of the proteomics findings is given in Table 1.

Decorin Processing in Cardiac Atria

On enrichment for glycoproteins, decorin peptides were consistently identified in the flowthrough (Figure 2A). Decorin has 3 consensus sequences for *N*-glycosylation at asparagine (Asn) 211, Asn262, and Asn303. Unlike other SLRPs, all *N*-glycosylation sites within decorin are located at the C-terminal half of the protein (Figure 2B). Glycosylation of decorin was confirmed by sequential deglycosylation and direct confirmation of its glycosylation sites by MS/MS (Table 1; Figure III in the online-only Data Supplement). A comparison of the sequence coverage revealed that only peptides from the nonglycosylated N-terminal half of decorin were identified in the flowthrough. In contrast, peptides spanning the entire sequence were obtained in the input and the glycoprotein-enriched fraction (Figure 2C). Trypsin is commonly used for protein digestion before MS/MS. Identification of cleavage sites produced by enzymes other than trypsin (nontryptic cleavages) can be indicative of proteolysis. Few ECM proteins displayed evidence for nontryptic cleavages (Table V in the online-only Data Supplement). For decorin, however, 18 cleavage sites were detected (Figure 3A), and 11.9% of all spectra were nontryptic (Figure IVA in the online-only Data Supplement). Despite >50% sequence homology to decorin, only 1.2% of spectra for biglycan were nontryptic. A sequence alignment between decorin and biglycan revealed that most

Table 1. Identification of ECM and ECM-Associated Proteins in Human Atrial Appendages

Proteins (97)	GuHCl (Input)	Glycoprotein Enrichment	Glycopeptide Analysis
Alpha-1-acid glycoprotein 1	+	+	
Alpha-1-acid glycoprotein 2		+	
Alpha-1B-glycoprotein	+	+	
Alpha-2-HS-glycoprotein		+	+
Annexin A2	+		
Apolipoprotein A-I	+		
Apolipoprotein A-IV	+		+
Apolipoprotein C-III	+		
Apolipoprotein E	+		
Asporin	+		
Basal cell adhesion molecule	+	+	+
Beta-2-glycoprotein 1	+	+	+
Biglycan	+		
Cadherin-13		+	
Cadherin-2	+	+	+
Cartilage intermediate layer protein 1		+	
Cartilage oligomeric matrix protein			+
Cathepsin G	+		
Chymase	+		
Clusterin	+	+	+
Collagen alpha-1(I)	+		
Collagen alpha-1(II)	+		
Collagen alpha-1(III)	+		
Collagen alpha-1(IV)	+		+
Collagen alpha-1(V)	+		
Collagen alpha-1(VI)	+		+
Collagen alpha-1(VIII)	+		
Collagen alpha-1(XV)	+		
Collagen alpha-1(XVIII)	+	+	
Collagen alpha-1(XXVIII)	+		+
Collagen alpha-2(I)	+		+
Collagen alpha-2(IV)	+		+
Collagen alpha-2(V)	+		
Collagen alpha-2(VI)	+		+
Collagen alpha-3(V)	+		
Collagen alpha-3(VI)	+	+	+
Collagen alpha-6(VI)		+	+
Decorin	+	+	+
Dermatopontin	+		
Dystroglycan	+		+
Elastin	+		
EMILIN-1			+
Extracellular superoxide dismutase	+		
Fibrillin-1	+	+	
Fibromodulin	+		
Fibronectin	+	+	
Fibulin-2		+	+
Galectin-1	+		
Galectin-3	+		
Galectin-3-binding protein	+	+	
Glypican-1	+		
Hepatoma-derived growth factor		+	
Insulin-like growth factor-binding protein 7		+	

(*Continued*)

Table 1. Continued

Proteins (97)	GuHCl (Input)	Glycoprotein Enrichment	Glycopeptide Analysis
Intercellular adhesion molecule 1		+	
Kininogen-1		+	
Lactadherin	+		
Laminin subunit alpha-2	+		
Laminin subunit alpha-4	+		
Laminin subunit alpha-5	+		
Laminin subunit beta-1	+		
Laminin subunit beta-2	+	+	+
Laminin subunit gamma-1	+	+	
Latent-TGFß-binding protein 2		+	
Latent-TGFß-binding protein 4		+	
Leukocyte elastase inhibitor	+		
Lumican	+	+	+
Mast cell carboxypeptidase A	+		
Matrix Gla protein	+		
Matrix-remodeling-associated protein 7		+	
Metalloproteinase inhibitor 3	+		
Mimecan	+	+	+
Natriuretic peptide A	+		
Neural cell adhesion molecule 1		+	
Neural cell adhesion molecule L1	+	+	+
Neutrophil defensin 1	+		
Nidogen-1	+	+	+
Nidogen-2	+	+	
Periostin	+		
Perlecan	+	+	
Podocan			+
Proactivator polypeptide		+	
Prolargin	+	+	+
Protein AMBP		+	
Proteoglycan 4		+	+
RPE-spondin		+	
Secreted frizzled-related protein 1	+		
Secreted phosphoprotein 24	+	+	
Serum amyloid P-component	+	+	+
Target of Nesh-SH3	+	+	
Tenascin		+	
Tenascin-X	+	+	+
TGFß-induced protein ig-h3	+		
Tryptase beta-2	+		
Tubulointerstitial nephritis antigen-like	+	+	
Versican	+	+	+
Vitronectin	+	+	+
Zinc-alpha-2-glycoprotein		+	

(*Continued*)

+ denotes identification by one of the three proteomics strategies

cleavage sites are within nonconserved regions (Figure IVB in the online-only Data Supplement), suggesting that sequence variation provides selectivity to the proteolytic processing of cardiac matricellular proteins.

Decorin Processing Is Region Specific

To investigate regional differences in decorin processing, decorin levels were compared between LAA and left ventricles (LVs). Antibodies raised against 3 different decorin regions were used: the N terminus (Ile36-Leu86), the internal part (Leu136-Ile215), and the C terminus (Phe312-Lys359) of decorin (Figure 3B). All 3 antibodies recognized recombinant human decorin, and decorin in human cardiac tissue, as well (Figure 3C). In agreement with its predicted relative molecular mass (Mr), decorin protein core migrated as a ≈45- to 48-kDa doublet after removal of the

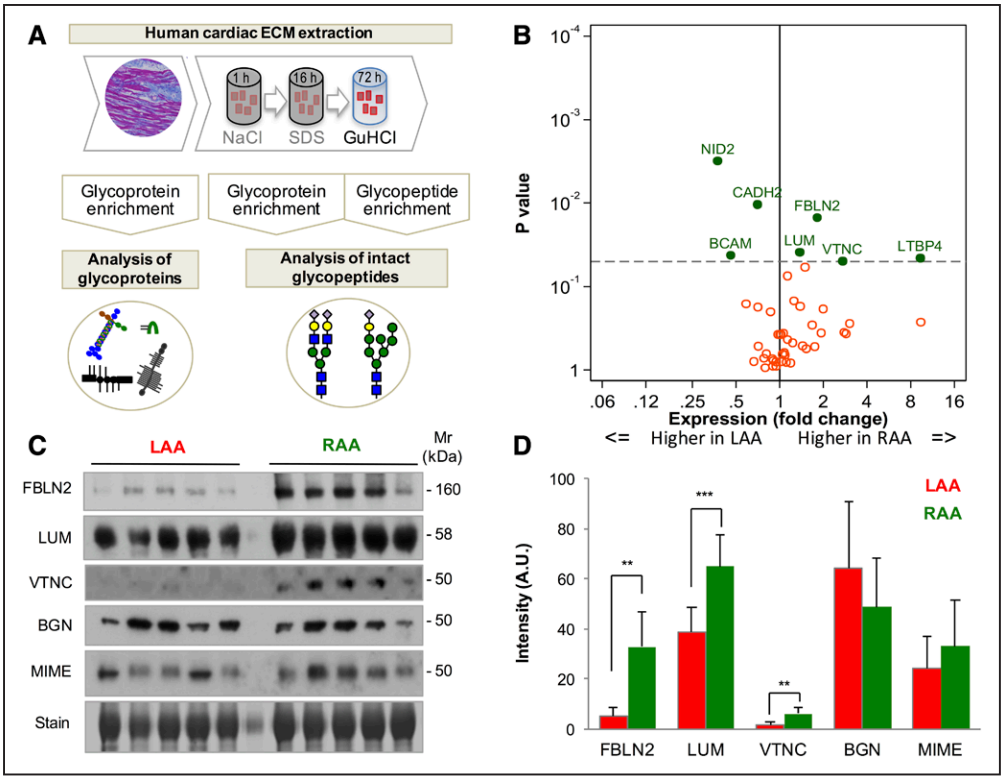

Figure 1. Glycoproteomics of the human cardiac ECM.
A, Atrial appendages were collected from patients in SR during cardiac surgery and subject to a decellularization-based 3-step extraction for ECM proteins. First, GuHCl extracts were analyzed by LC-MS/MS. Then, ECM extracts were enriched for glycoproteins. The glycoprotein-enriched and unbound flowthrough fractions were analyzed by LC-MS/MS. Finally, enrichment was performed for glycoproteins, and glycopeptides, as well, for direct glycopeptide identification by LC-MS/MS. **B,** Comparison of ECM-related glycoproteins in LAA and RAA (n=5, each). **C,** Validation by immunoblotting. Biglycan, mimecan (MIME), and Coomassie staining were included as controls. **D,** Quantification by densitometry. Bars represent mean±SD. $^{**}P<0.01$. $^{***}P<0.001$. A.U. indicates arbitrary units; BCAM, basal cell adhesion molecule; CADH2, cadherin 2; ECM, extracellular matrix; FBLN2, fibulin 2; GuHCl, guanidine hydrochloride; LAA, left atrial appendage; LC-MS/MS, liquid chromatography-tandem mass spectrometry; LTBP4, latent transforming growth factor-β binding protein 4; LUM, lumican; NID2, nidogen 2; RAA, right atrial appendage; SD, standard deviation; SDS, sodium dodecyl sulfate; SR, sinus rhythm; and VTNC, vitronectin.

glycosaminoglycan chain, but the 3 antibodies provided 3 different results (Figure 3C): according to the antibody recognizing the C terminus, decorin was reduced in LAA in comparison with LV. The antibodies to the internal and the N-terminal part of decorin, however, did not confirm this result, but revealed a Mr difference of ≈3 kDa between decorin in LAA (45 kDa) and LV (48 kDa). C-terminal truncation of decorin may explain this apparent discrepancy. The C-terminal region of decorin inhibits the activity of CTGF. At the protein level, CTGF was more abundant in LV than LAA (Figure 3C, bottom) despite reduced transcript levels (Figure VA in the online-only Data Supplement). A search for putative protease targets on decorin using the PROSPER database returned cathepsins K and G as the most likely effectors (Figure VB in the online-only Data Supplement) for the prominent cleavage at the C terminus observed at Phe330-Ser331 (Figure IVB in the online-only Data Supplement). Transcript levels for cathepsin K were higher in LAA than in LV (Figure VC in the online-only Data Supplement). Taken together, these data suggest region-specific processing of decorin in the human cardiac ECM that may affect the local retention of growth factors.

Decorin Cleavage in AF

AF, the most common arrhythmia encountered in clinical practice, results in significant morbidity and mortality. To provide insight into the consequences of persistent AF on decorin protein abundance, we compared LAA from patients in sinus rhythm (SR) with those with postoperative AF (SR-AF) and in persistent AF (Figure 4A, Figure VIA in the online-only Data Supplement). Tables VI and VII in the online-only Data Supplement summarize their clinical characteristics. At the transcript level, there was no change of decorin or CTGF expression in AF patients and patients who developed postoperative AF in comparison with SR controls (Figure VIB in the online-only Data Supplement). At the protein level, however, the structural damage inflicted by prolonged AF was associated with higher levels of the full-length and the 45-kDa forms of decorin (Fig-

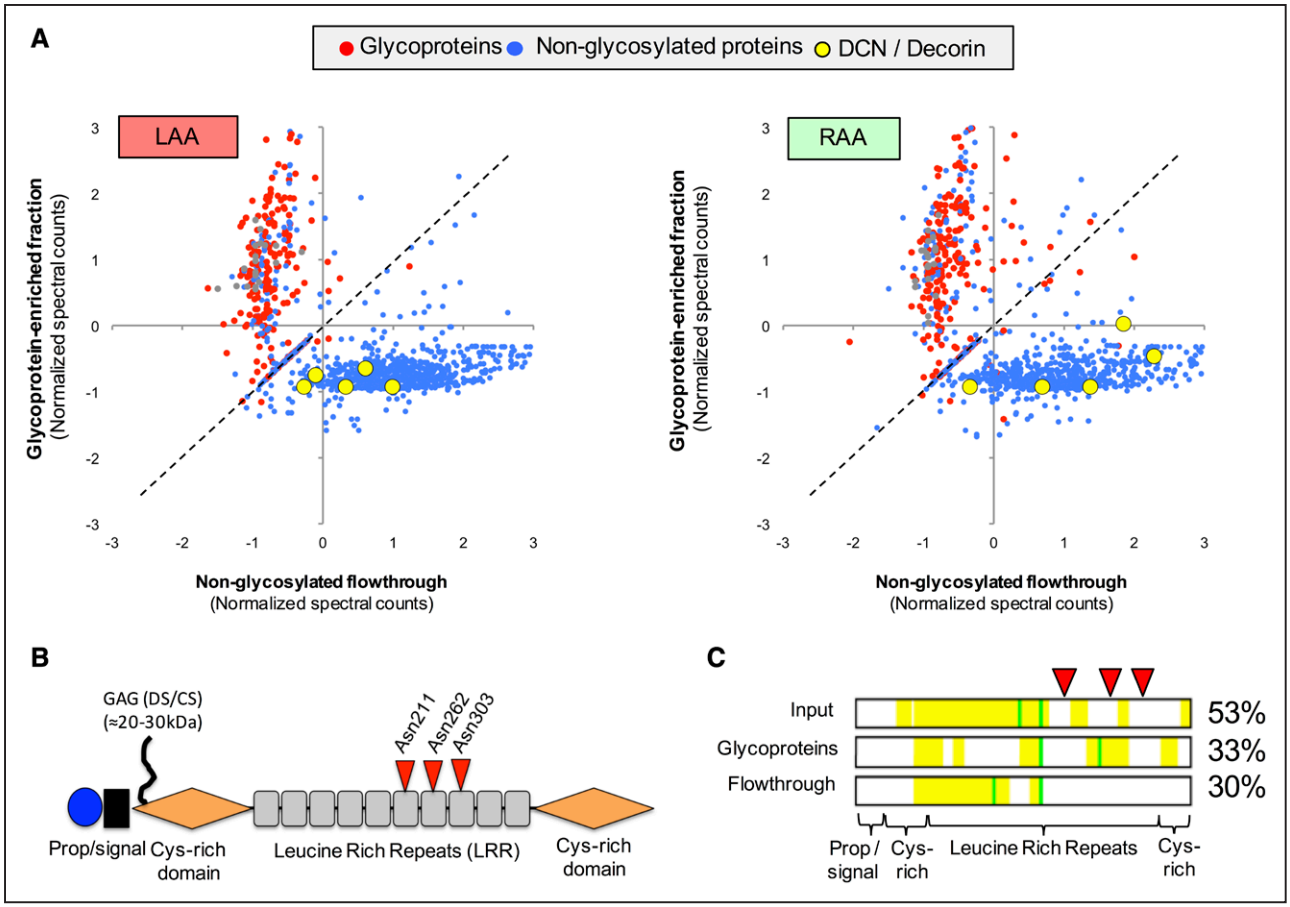

Figure 2. Decorin after glycoprotein enrichment.

A, Proteomic comparison of the glycoprotein-enriched fraction and the flowthrough. Relative abundances of glycoproteins (red dots) and nonglycosylated proteins (blue dots) are plotted for LAA and RAA (n=5, each). Decorin was the only glycoprotein consistently detected among the nonglycosylated proteins in the flowthrough (yellow dots). **B,** The C-terminal half of decorin has 3 *N*-glycosylation sites (red triangles). **C,** According to the sequence coverage (yellow color) in the 3 different fractions (input, glycoprotein-enriched fraction, and nonglycosylated flowthrough), only N-terminal (nonglycosylated) decorin peptides were identified in the flowthrough. DCN indicates decorin; LAA, left atrial appendage; and RAA, right atrial appendage.

ure 4B). The shift in the Mr by 3 kDa was similar to the one previously observed in LVs. Notably, CTGF protein levels were concurrently enhanced (Figure VIC in the online-only Data Supplement). Gene expression data using primers for the different regions of decorin support the notion that the processing of decorin occurs at the protein rather than the transcriptional level (Figure VID in the online-only Data Supplement). In contrast, decorin protein levels were found to be reduced in the SR-AF cohort in comparison with patients who maintained SR postoperatively (SR-SR) (Figure VII in the online-only Data Supplement).

Next, we interrogated the MS/MS data for potential cleavage sites.[12] Nontryptic peptides of decorin predominantly originated from 4 sites: Val65-Gln66, Leu79-Pro80, Ser121-Pro122, and Phe330-Ser331. The latter cleavage site provides an explanation for the loss of detection with the antibody recognizing C-terminal epitopes. MS/MS spectra are shown in Figure VIIIA in the online-only Data Supplement, alongside elution times for the corresponding tryptic and nontryptic peptides to exclude in-source fragmentation. Notably, an additional cleavage site (Ser49-Leu50) was found in AF (Figure 4C). This cleavage site is next to an N-terminal domain that inhibits myostatin,[11] a negative regulator of muscle cell growth. According to the absolute and relative intensities (Figure VIIIB in the online-only Data Supplement), the nontryptic decorin peptide generated by proteolytic cleavage at Ser49-Leu50 was higher in AF patients. Structurally, this part of decorin constitutes a natively disordered region,[13] which hindered further assessment of putative protease cleavage sites[14] (Figure IX in the online-only Data Supplement).

Inhibition of Myostatin Activity

Myostatin gene expression was significantly reduced in AF patients (Figure 5A). Thus, we hypothesized that this processed form of decorin protein core generated dur-

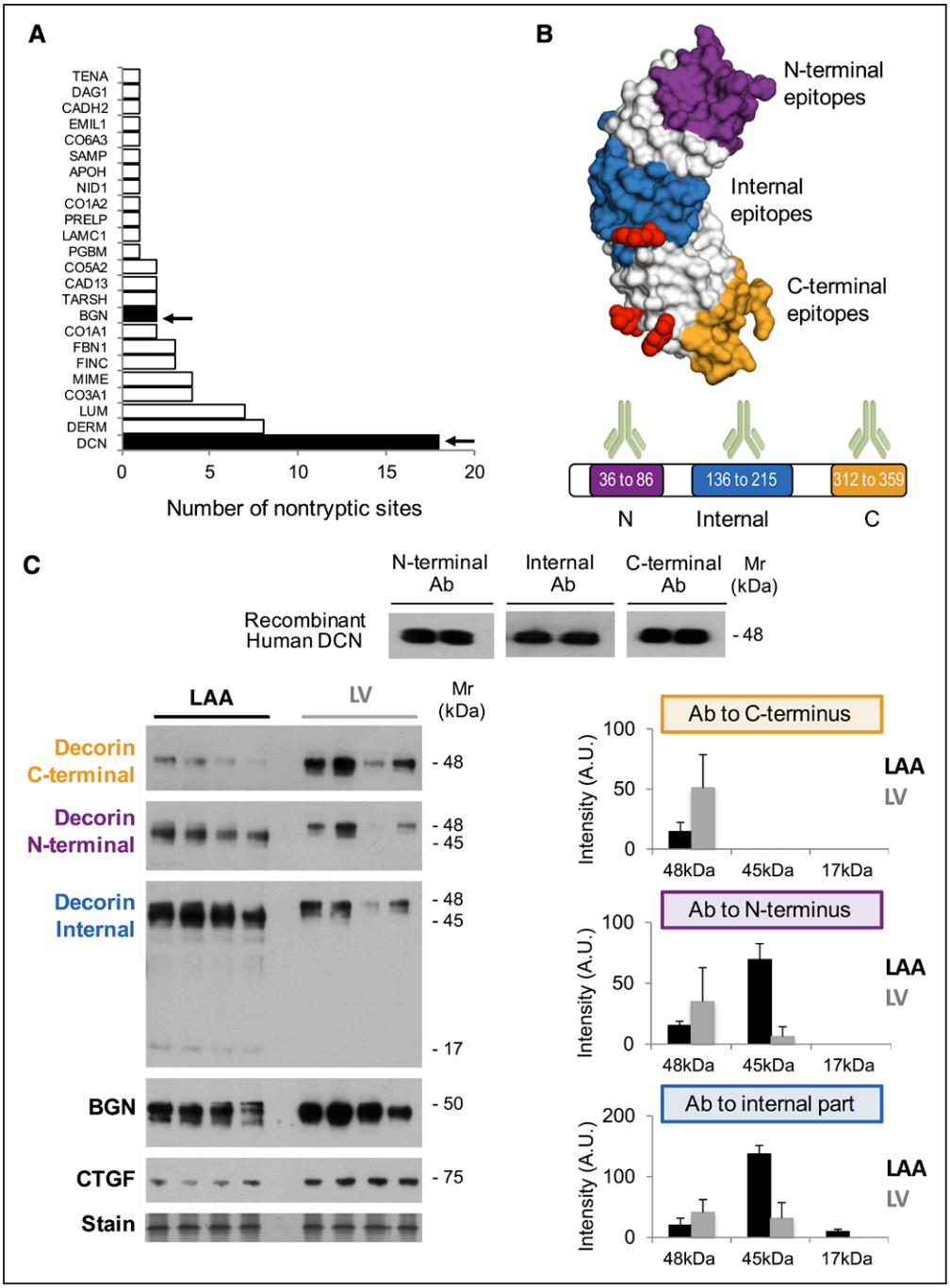

Figure 3. Decorin processing in atrial tissue.

A, Decorin (DCN) showed the greatest number of nontryptic cleavage sites among all ECM proteins identified. Biglycan (BGN) is highlighted for comparison. **B,** Three different antibodies recognizing different epitopes were used to detect decorin. Numbers indicate amino acid positions. **C,** Comparison of LAA and LV. Note the C-terminal truncation of decorin in LAA in comparison with LV from nonfailing hearts (Mr shift from 48 kDa to 45 kDa). The apparent reduction of decorin levels in LAA with the C-terminal antibody was not corroborated by antibodies to N-terminal and internal epitopes. Instead, they revealed a loss of ≈3 kDa in LAA in comparison with LV. Biglycan, a highly homologous SLRP, showed no such shift in Mr. The graphs show the densitometry results from immunoblots based on antibodies against 3 different decorin epitopes. Bars represent mean±SD. Ab indicates antibody; A.U, arbitrary units; CTGF, connective tissue growth factor; ECM, extracellular matrix; LAA, left atrial appendage; LV, left ventricle; Mr, relative molecular mass; SD, standard deviation; and SLRP, small leucine-rich proteoglycan.

ing AF could directly interfere with myostatin bioactivity. Myostatin inhibits phosphorylation of AMP-activated protein kinase (AMPK) and activates SMAD2/3 (Figure 5B). Via the SMAD2/3 cascade, myostatin controls cell growth and differentiation. By inhibiting AMPK phosphorylation, myostatin alters cardiac metabolism.

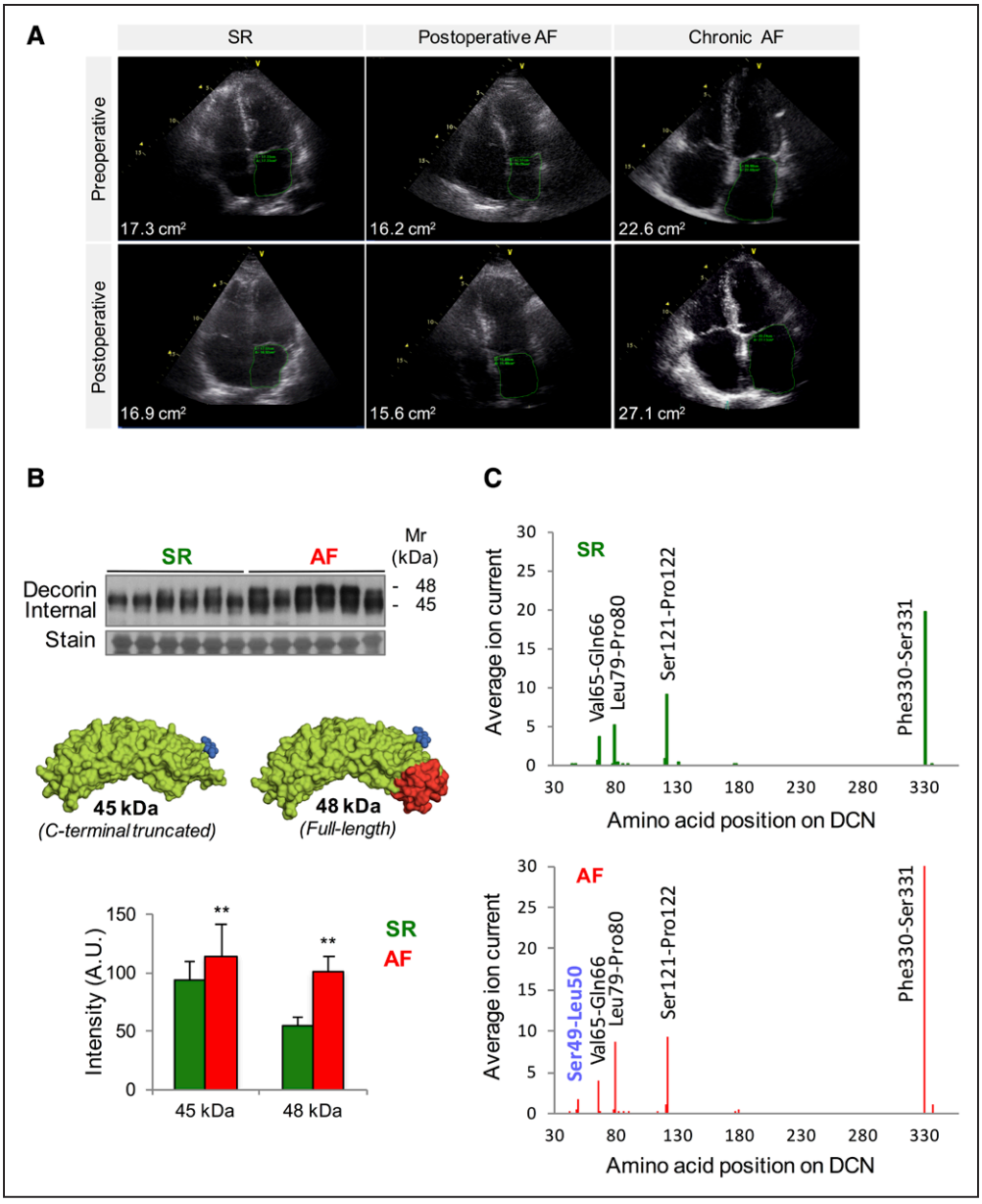

Figure 4. Decorin processing in AF.

A, Representative preoperative and postoperative echocardiography images from patients who stayed in SR throughout surgery and patients who developed postoperative AF. Rightmost images depict left atrial structural remodeling observed in a patient with permanent, chronic AF after a 5-year follow-up. **B,** Immunoblotting for decorin in GuHCl extracts from LAA samples. Decorin was more abundant in AF than SR patients, and both bands (C-terminally truncated decorin at 45 kDa and full-length at 48 kDa) became detectable. The bottom chart shows the quantification (mean±SD) in SR and AF patients (n=6, each) with the antibody against the internal region. $^{**}P<0.01$. **C,** GuHCl extracts (n=6, each group) were analyzed using LC-MS/MS. After a search using no enzyme, nontryptic decorin peptides were identified and quantified. In addition to the 4 main cleavage sites of decorin in SR, a N-terminal cleavage site at position Ser49-Leu50 was detected in AF. AF indicates atrial fibrillation; A.U, arbitrary units; GuHCl, guanidine hydrochloride; LAA, left atrial appendage; LC-MS/MS, liquid chromatography-tandem mass spectrometry; SD, standard deviation; and SR, sinus rhythm.

We synthesized peptides corresponding to the N-terminal peptides of mouse and human decorin (Figure XA in the online-only Data Supplement) and tested their activity in a reporter gene assay using HEK293 cells transfected with CAGA-luciferase plasmid. CAGA boxes are recognized by SMAD3 on the promoter regions of SMAD3-responsive genes, and therefore this technique screens SMAD3 activity. Incubation of transfected cells with 2.5 nmol/L myostatin triggered the activation of pathways downstream of the myostatin receptor as evidenced by increased luciferase activity. Addition of the synthetic N-terminal peptide (murine decorin amino

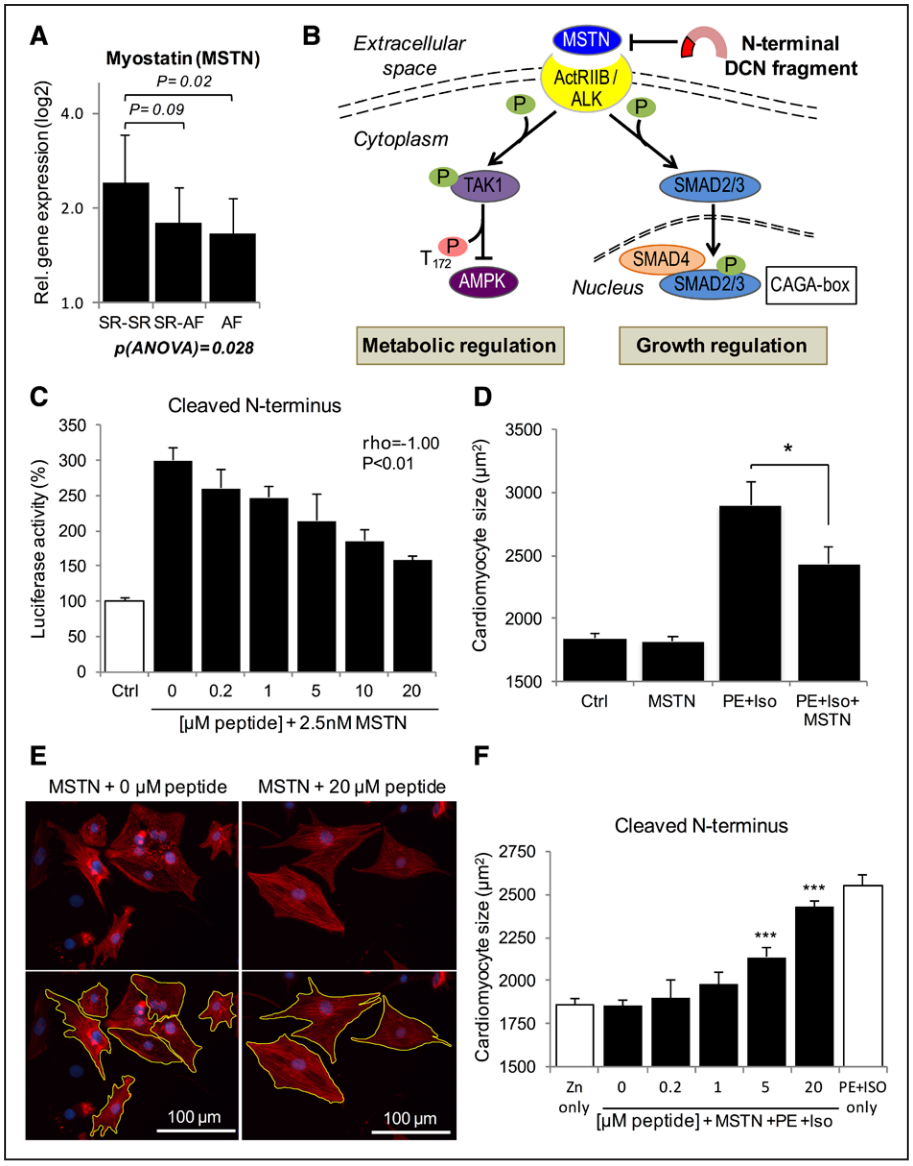

Figure 5. Decorin peptides bind myostatin.

A, qPCR analysis for myostatin expression in additional samples (SR-SR=14, SR-AF=10, AF=13). Bars represent mean±SD. **B,** Schematic illustration of 2 downstream signaling pathways of myostatin (MSTN). ActRIIB/ALK denotes activin receptor type-2B (ActRIIB)/ activin receptor-like kinase (ALK) receptor complex; and TAK1, transforming growth factor β-activated kinase 1. **C,** Repression of MSTN-SMAD3 signaling. A synthetic N-terminal peptide of mouse decorin (amino acids 42–71 corresponding to the peptide generated by the Ser49-Leu50 cleavage site in humans) inhibited the CAGA-luciferase reporter activity in a dose-dependent manner. The trend for the effect was calculated based on Spearman correlation (ρ). Bars are mean±SD of triplicate experiments. **D,** Effect on rat cardiomyocytes. MSTN represses hypertrophy induced by pretreatment with isoproterenol (Iso) and phenylephrine (PE). Cardiomyocyte size is given as mean±standard error of the mean (SEM). **E,** Cardiomyocyte size was calculated after defining the cell perimeter to integrate the area (see bottom images). **F,** The decorin N-terminal peptide attenuated the MSTN effect dose-dependently (0–20 µmol/L). Cardiomyocyte size is given as mean±SEM based on a total of 300 to 400 cell measurements per experimental condition and compared with a control without decorin N-terminal peptide. **P*<0.05. ****P*<0.001. AF indicates atrial fibrillation; ANOVA, analysis of variance; DCN, decorin; qPCR, quantitative polymerase chain reaction; SR, sinus rhythm; and SR-AF, postoperative AF.

acids 42–71, cleaved N terminus) dose-dependently reduced this response (ρ=–1.00, *P*<0.01) (Figure 5C). A longer decorin peptide (mouse amino acids 31–71, full N terminus) was not as effective (ρ=–0.83, *P*=0.04) (Figure XB in the online-only Data Supplement). Next, cell size was measured on isolated neonatal rat cardiomyocytes (Figure 5D). The shorter N-terminal peptide mediated a strong repression of myostatin activity as evidenced by an increase in cell size on hypertrophy stimuli (ie, isoproterenol and phenylephrine) (Figure 5E

and 5F; Figure XC in the online-only Data Supplement). Thus, decorin cleavage generates peptides with antimyostatin activity.

Decorin Null Mice

The interaction of decorin with myostatin was further confirmed in hearts obtained from decorin null ($DCN^{-/-}$) mice. Decorin deficiency resulted in a ≈50% reduction of myostatin expression (Figure 6A). Related ECM proteins showed no changes in abundance, but decorin deficiency was accompanied by a marked increase in SMAD2 phosphorylation (Figure 6B). Metabolic consequences of decorin deficiency were evident in metabolic profiles obtained by $^{+}$H-NMR spectroscopy (Figure 6C; Figure XIA in the online-only Data Supplement). Levels of glutamine, succinate, aspartate, and nicotinamide adenine dinucleotides (NAD^{+}, NADH) were elevated in decorin null hearts, in comparison with littermate controls (Figure 6D). In isolated cardiomyocytes, myostatin reduced AMPK phosphorylation, a master regulator for cardiac energy metabolism (Figure 6E). This myostatin effect was reversed by preincubation with decorin peptides corresponding to the myostatin-binding region in mice and humans (Figure 6F; Figure XIB and XIC in the online-only Data Supplement). A similar inhibitory effect of the N-terminal decorin peptide on myostatin signaling was observed in Langendorff hearts (Figure 6G and 6H; Figure XID in the online-only Data Supplement).

DISCUSSION

By applying a novel proteomics approach to human atria, fundamental insights were obtained about the composition and the proteolytic processing of the human cardiac ECM, which has not been analyzed by proteomics thus far. Using proteomics in combination with metabolomics, we have previously shown that discordant metabolic alterations are evident in individuals susceptible to postoperative AF.[4] We now identify endogenous decorin cleavage products in AF that may contribute to atrial remodeling and play a previously unrecognized role in the susceptibility or perpetuation of arrhythmias by altering the local bioavailability of growth factors, such as CTGF and myostatin.

Glycoproteomics of the Cardiac ECM

Thus far, proteomic studies of cardiac disease have focused mainly on evaluating the differences in protein abundance,[4,5] phosphorylation,[9,15] and redox modifications.[16] However, alterations in glycosylation patterns and protein degradation are known to occur in disease.[17] Our study characterizes, for the first time, ECM proteins in human atria by using state-of-the-art glycoproteomics. Previously, Parker et al[18] used glycoproteomics in rat hearts and characterized glycan composition after removal of the sugar moieties from the peptides. In this study, we analyzed intact glycopeptides. Unlike conventional studies, in which ECM proteins are analyzed by antibodies, proteomics does not require a priori decisions on which ECM proteins to study, and MS/MS is not dependent on the recognition of epitopes. Epitopes can become masked, ie, by glycosylation or be rendered undetectable by proteolytic cleavage. These inherent constraints of antibody-based detection can lead to misinterpretations as demonstrated by the 3 immunoblots for decorin presented in Figure 3C.

Decorin and Other SLRPs

Decorin is a member of SLRPs, a family of 18 structurally related ECM proteins. After synthesis, SLRPs are secreted into the extracellular space and exert diverse roles as biologically active regulators of the ECM.[19] Similar to biglycan, decorin has a horseshoe shape and binds to collagen fibers to control their shape, size, and distribution. Decorin and biglycan share >50% sequence identity and have chemically similar amino acid substitutions at most other positions.[20] Yet, decorin, but not biglycan, was subject to extensive proteolytic processing in human atria. Despite the structural and functional similarities of SLRPs, decorin is located in the interstitial ECM, whereas biglycan is mainly associated to collagens in the pericellular regions.[21] A sequence alignment between decorin and biglycan revealed that most cleavage sites in decorin mapped to nonconserved regions. Thus, specific cleavage sites might endow decorin with additional functional properties in the heart.

Biological Activity of ECM Cleavage Products

Besides its role in ECM assembly, decorin has structural moieties that recognize not only collagens, but also growth factors and cell surface receptors, affecting their activity and bioavailability.[19,22] The regulatory mechanisms involve interactions with sugar residues or specific domains within the core protein.[23] It is noteworthy that, among all SLRPs, decorin had the greatest number of nontryptic cleavage sites, which were predominantly located on the N-terminal half of the protein. In general, the N-terminus and the C-terminus of SLRPs offer the greatest variability for interaction partners.[22] The decorin peptides within the N-terminal half have antimyostatin properties.[11] An abundant cleavage site at the C-terminus (Phe330-Ser331) gives rise to a peptide with CTGF-binding properties.[24] The known cleavage sites of decorin, and the nontryptic cleavages identified in atrial appendages and their relation to binding sequences for collagen and growth factors,

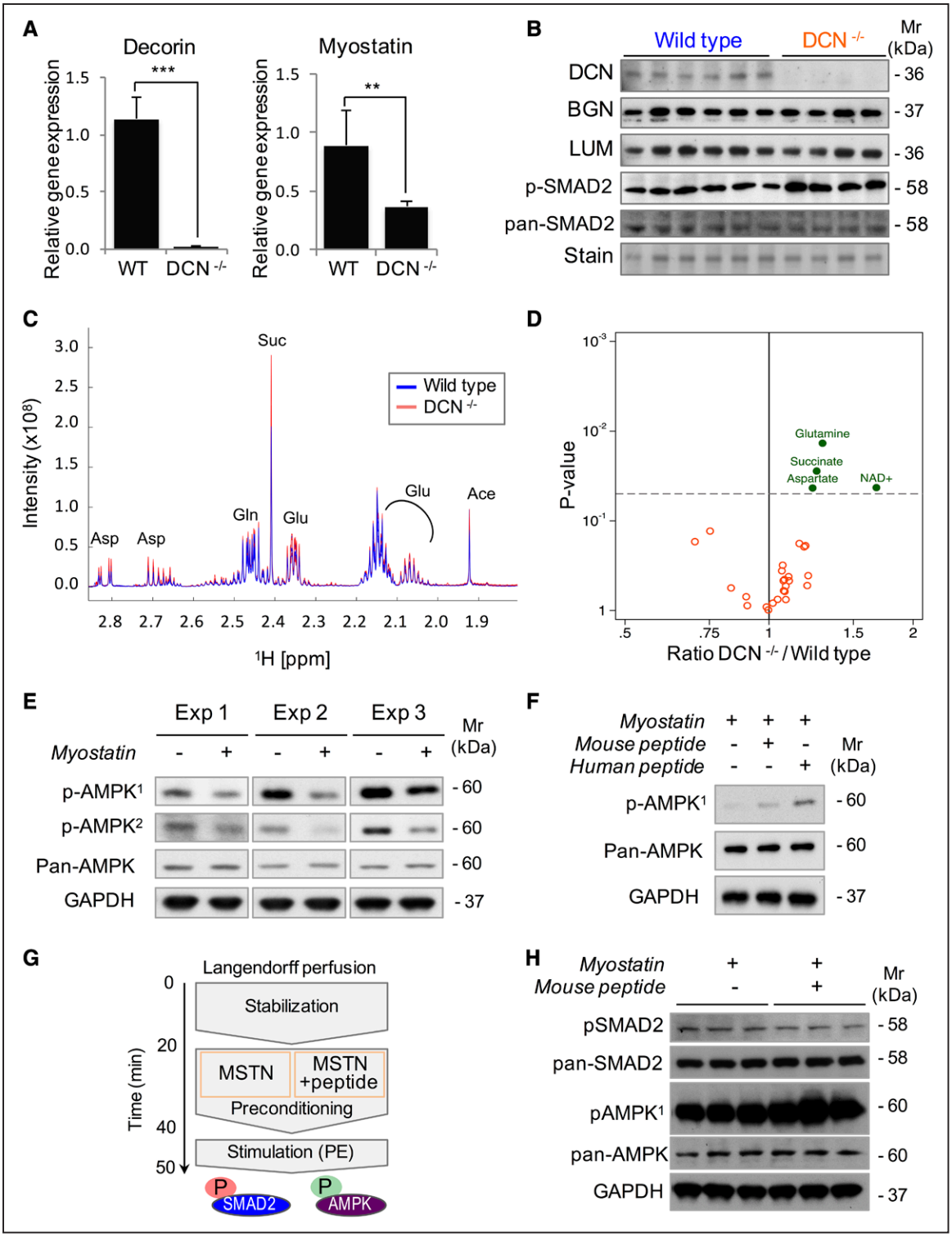

Figure 6. Effect of decorin on cardiac metabolism.

A, Deficiency of decorin was associated with reduced expression of myostatin in murine hearts. Bars represent mean±SD. **B,** In hearts of decorin null mice, the abundance of closely related SLRPs, such as biglycan and lumican (LUM), was not affected, but phosphorylation of SMAD2 was increased. **C,** Overlay of $^{+}$H-NMR spectra from wild-type and decorin null (DCN$^{-/-}$) hearts. **D,** Metabolic profiles of cardiac tissue from DCN$^{-/-}$ mice revealed elevated levels of glutamine (Gln), succinate (Suc), aspartate (Asp), and nicotinamide adenine dinucleotides (NAD^{+}, NADH). **E,** Myostatin represses AMPK activation in rat cardiomyocytes. Immunoblotting was performed with 2 different antibodies for AMPK phospho-Thr$_{172}$. Levels of total AMPK (pan-AMPK) were unchanged. **F,** N-terminal decorin peptides from mouse or human origin (20 μmol/L) reversed the effect of myostatin on AMPK phosphorylation. Rat cardiomyocytes were stimulated with Iso and PE after incubation with myostatin for 2 hours. **G,** Schematic (*Continued*)

as well, are summarized in Figure XII in the online-only Data Supplement.

C-Terminal Decorin Peptides Bind CTGF

The C-terminal tail of decorin, also known as the cysteine-rich ear, is involved in ligand-binding regulation and conformational stability via 2 cysteines at positions 313 and 346. A point mutation within this region is the genetic cause for congenital hereditary stromal dystrophy of the cornea and linked to abnormal fibrillogenesis.[25] The abundant cleavage site at position Phe330-Ser331 results in a truncated form of decorin (loss of 3 kDa). C-Terminal truncation of decorin was predominantly observed in LAA and to a lesser extent in LV. Importantly, a synthetic decorin peptide within LRR12 (ie, Gln335-Lys359) has been shown to bind CTGF and attenuate fibrosis.[24] Thus, C-terminal truncation may result in diminished collagen-binding ability and repression of CTGF activity in human atria with their lower mechanical load and decreased stiffness compared to LV (Figure 7).

N-Terminal Decorin Peptides Regulate Myostatin

At the N terminus, 4 cysteine residues form a disulfide knot (Cys54-Cys60 and Cys58-Cys67) that buries the hydrophobic core of the first leucine-rich repeat (LRR1). The binding of Zn^{2+} to this region results in a conformational change required for myostatin binding.[26] Equivalent biglycan moieties do not bind myostatin.[26,27] Myostatin, a potent antagonist to hypertrophic stimuli,[28] is synthesized as inactive protein with a N-terminal propeptide. After activation, myostatin is regulated via noncovalent binding to its propeptide, forming a latent complex.[29] Our experiments demonstrated a markedly lower expression of myostatin in hearts of decorin null mice, supporting the notion of a myostatin-decorin feedback loop. In cardiomyocytes, myostatin regulates at least 2 pathways downstream of the activin receptor (Figure 5B): (1) Coincubation of myostatin with the N-terminal decorin peptide led to inhibition of SMAD2/3 activity in a dose-dependent manner. SMAD3 activation via myostatin represses muscle cell growth.[30] When cardiomyocytes were treated with increasing concentrations of the N-terminal decorin peptide, the effect of myostatin on cell size was reversed. In line with these in vitro findings, SMAD2 phosphorylation was increased in hearts of decorin null mice. (2) By inhibiting AMPK phosphorylation via activin receptor and TAK1, myostatin regulates cardiac energy homeostasis.[31] AMPK is a crucial energy sensor with a phosphorylation site in its activation loop at threonine 172 (Thr_{172}).[32] In in vitro and ex vivo experiments, both the murine and the human N-terminal peptides of decorin maintained phosphorylation of AMPK at Thr_{172} in the presence of myostatin. In hearts of decorin null mice, with reduced myostatin levels, NMR spectroscopy profiling revealed changes in metabolites linked to mitochondrial metabolism and an accumulation of nicotinamide adenine dinucleotides. Activation of AMPK increases ATP production mostly by enhancing oxidative metabolism leading to a gradual increase in NAD^+ levels as a consequence of fatty acid oxidation.[33]

Decorin in Patients With AF

In human AF, we observed an additional decorin cleavage site next to the myostatin-binding region (Figure 7, position Ser49-Leu50).[11] This cleavage site generates a decorin form devoid of the glycosaminoglycan chain at Ser34.[14] We demonstrated that the resulting peptide suppresses myostatin activity and increases cardiomyocyte size. Notably, in a goat model of pacing-induced AF, changes in cellular substructures were accompanied by an increase in myocyte size (up to 195%).[34] The additional cleavage site in AF releases decorin peptides that only contain the myostatin-binding region and are therefore less likely to interact with other binding partners. In comparison with other regulators of myostatin activity, ie, myostatin propeptide and follistatin,[35] decorin is abundant and readily available within the cardiac ECM. Thus, its cleavage products may constitute an important local regulatory mechanism of myostatin activity.

Evidence in Preclinical Models

Inhibition of myostatin by cardiac-specific overexpression of the myostatin propeptide induced enlarged atria and AF in the transgenic mice.[36] Similarly, mice overexpressing microRNA-208a, a myomiR enriched in hearts, developed spontaneous AF. Besides thyroid hormone receptor–associated protein 1, myostatin was identified as a regulatory target of microRNA-208a.[37] Similarly, AMPK signaling, one of the key downstream signaling pathways of myostatin, has been implicated as a mechanism for AF in mice with cardiac-specific deletion of liver kinase B1.[38] Taken together, these data provide in vivo evidence

Figure 6 Continued. summary of the experiment in Langendorff perfused mouse hearts. **H,** Phosphorylation levels of AMPK and SMAD2 were used as readouts for inhibition of myostatin signaling by the N-terminal decorin peptide. $^{**}P<0.01$. $^{***}P<0.001$. AMPK indicates AMP-activated protein kinase; MSTN, myostatin; NMR, nuclear magnetic resonance; SD, standard deviation; SLRP, small leucine-rich proteoglycan; and WT, wild type.

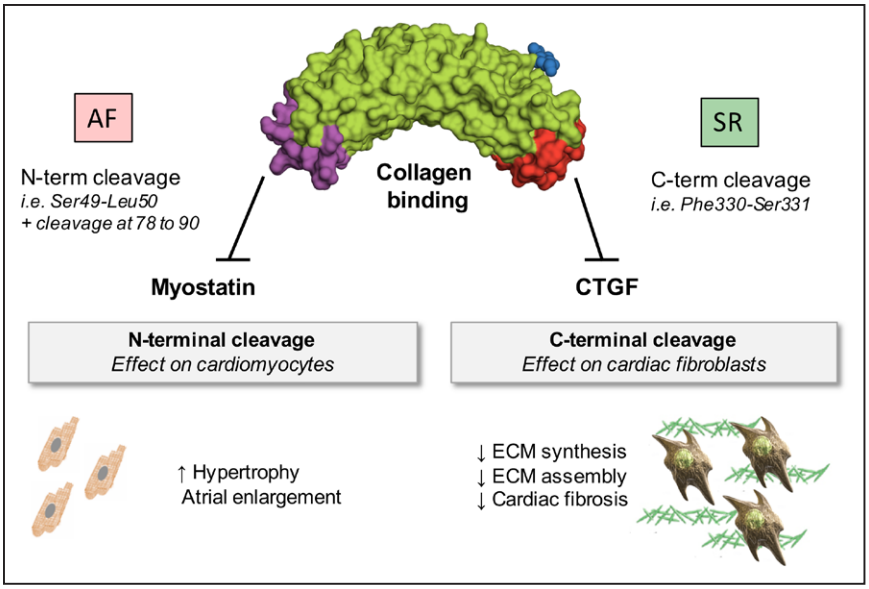

Figure 7. Decorin in human atria. Decorin cleavage constitutes a mechanism for local regulation of growth factor bioactivity in the human cardiac ECM. N-terminal cleavage of decorin was observed in patients with persistent AF and gives rise to peptides with antimyostatin activity. C-terminal truncation is more common in atria than ventricles and releases the CTGF-binding domain of decorin. AF indicates atrial fibrillation; CTGF, connective tissue growth factor; ECM, extracellular matrix; SR, sinus rhythm; and term, terminal.

that loss of myostatin activity and dysregulation of AMPK signaling can act as a substrate for AF, at least in mice.

Study Limitations

Our proteomics findings in clinical samples do not directly prove a decorin-mediated effect on atrial myostatin signaling. Although local injection of decorin peptides in skeletal muscle increased muscle mass,[11] in vivo studies are required to further explore the role of decorin cleavage products in cardiac disease, ie, the specificity of the interaction and the location of the effects. Decorin has many binding partners.[8] Thus, the genetic deletion of decorin in mice may have pleiotropic effects. Lectin enrichment of glycoproteins introduces a selectivity bias toward specific glycoforms, and high Mr glycoproteins in basement membranes, ie, collagens, laminins, and perlecan, are barely resolubilized by buffers compatible with the affinity enrichment of glycoproteins. The direct glycopeptide method used in this study identifies the peptide sequence, the glycosite, and the glycan mass, but the glycan composition is only calculated based on accurate mass and the glycan structure remains unresolved. Emerging technologies combining MS with glycan structural data are yet to be applied to human cardiac tissue.[39] Moreover, nontryptic cleavage sites at positions containing lysine or arginine will be missed by digestion with trypsin. Advances in positional proteomics will help to better characterize proteolytic cleavage in cardiac disease.[40]

Conclusions

The glycoproteomic analysis of atrial appendages allowed, for the first time, a detailed analysis of human cardiac ECM proteins. It examined differences in the ECM composition between RAA and LAA, confirmed putative and revealed new glycosylation sites in the cardiac ECM, and identified decorin-derived cleavage products that can act as local regulators of growth factor activity. Proteomic workflows, as outlined in this study, will be essential to explore the different aspects of ECM remodeling in cardiovascular disease, as exemplified by the observed changes in decorin processing during structural remodeling in persistent AF.

SOURCES OF FUNDING

Prof Mayr is a Senior Research Fellow of the British Heart Foundation (FS/13/2/29892). Dr Zampetaki is an Intermediate Research Fellow of the British Heart Foundation. Dr Willeit is an Erwin Schrödinger Fellow in Epidemiology sponsored by the Austrian Science Fund (J 3679-B13). Prof Fischer obtained funding from the Deutsche Forschungsgemeinschaft (DFG/SFB 1116). Prof Thum was supported by the ERC Consolidator Grant Longheart. Prof Mayr and Prof Thum have joint funding from the Leducq Foundation (MIRVAD). This work was supported by King's British Heart Foundation Center and the National Institute for Health Research (NIHR) Biomedical Research Center based at Guy's and St Thomas' NHS Foundation Trust and King's College London in partnership with King's College Hospital. There is no relationship with industry.

DISCLOSURES

None.

AFFILIATIONS

From King's British Heart Foundation Centre, King's College London, United Kingdom (J.B.-B., A. Zoccarato, R.K.-T., M.F., X.Y., A. Zampetaki, M.C., P.W., A.M.S., K.O., M.M.); Institute for Molecular and Translational Therapeutic Strategies, MH-Hannover, Germany (S.K.G., T.T.); St George's Hospital, NHS Trust,

London, United Kingdom (M.F., A.V., A.K., M.J.); University Medical Center Hamburg-Eppendorf, Germany (T.W., M.N.H.); Protein Metrics, San Carlos, CA (M.B.); Biobanco A Coruña, INIBIC-Complexo Hospitalario Universitario de A Coruña, Spain (N.D.); Institut für Allgemeine Pharmakologie und Toxikologie, Klinikum der Goethe-Universität Frankfurt, Frankfurt am Main, Germany (L.S.); Institute for Pharmacology and Clinical Pharmacology, Heinrich-Heine-University, Düsseldorf, Germany (J.W.F.); Sidney Kimmel Medical College at Thomas Jefferson University, Philadelphia, PA (R.V.I.); Thermo Fisher Scientific, San Jose, CA (R.V.); Experimental Cardiology, Department of Cardiology and Angiology, MH-Hannover, Germany (J.H.); and Laboratoire Vecteurs: Synthèse et Applications Thérapeutiques, UMR 7199 CNRS Université de Strasbourg, Illkirch, France (A.K.).

FOOTNOTES

Received May 17, 2014; accepted June 27, 2016.

The online-only Data Supplement is available with this article at http://circ.ahajournals.org/lookup/suppl/doi:10.1161/CIRCULATIONAHA.115.016423/-/DC1.

Circulation is available at http://circ.ahajournals.org.

REFERENCES

1. Pellman J, Lyon RC, Sheikh F. Extracellular matrix remodeling in atrial fibrosis: mechanisms and implications in atrial fibrillation. *J Mol Cell Cardiol*. 2010;48:461–467. doi: 10.1016/j.yjmcc.2009.09.001.
2. Dawson K, Wakili R, Ordög B, Clauss S, Chen Y, Iwasaki Y, Voigt N, Qi XY, Sinner MF, Dobrev D, Kääb S, Nattel S. MicroRNA29: a mechanistic contributor and potential biomarker in atrial fibrillation. *Circulation*. 2013;127:1466–75, 1475e1. doi: 10.1161/CIRCULATIONAHA.112.001207.
3. Chiang DY, Lebesgue N, Beavers DL, Alsina KM, Damen JM, Voigt N, Dobrev D, Wehrens XH, Scholten A. Alterations in the interactome of serine/threonine protein phosphatase type-1 in atrial fibrillation patients. *J Am Coll Cardiol*. 2015;65:163–173. doi: 10.1016/j.jacc.2014.10.042.
4. Mayr M, Yusuf S, Weir G, Chung YL, Mayr U, Yin X, Ladroue C, Madhu B, Roberts N, De Souza A, Fredericks S, Stubbs M, Griffiths JR, Jahangiri M, Xu Q, Camm AJ. Combined metabolomic and proteomic analysis of human atrial fibrillation. *J Am Coll Cardiol*. 2008;51:585–594. doi: 10.1016/j.jacc.2007.09.055.
5. Barallobre-Barreiro J, Didangelos A, Schoendube FA, Drozdov I, Yin X, Fernández-Caggiano M, Willeit P, Puntmann VO, Aldama-López G, Shah AM, Doménech N, Mayr M. Proteomics analysis of cardiac extracellular matrix remodeling in a porcine model of ischemia/reperfusion injury. *Circulation*. 2012;125:789–802. doi: 10.1161/CIRCULATIONAHA.111.056952.
6. Jahanyar J, Joyce DL, Southard RE, Loebe M, Noon GP, Koerner MM, Torre-Amione G, Youker KA. Decorin-mediated transforming growth factor-beta inhibition ameliorates adverse cardiac remodeling. *J Heart Lung Transplant*. 2007;26:34–40. doi: 10.1016/j.healun.2006.10.005.
7. Melchior-Becker A, Dai G, Ding Z, Schäfer L, Schrader J, Young MF, Fischer JW. Deficiency of biglycan causes cardiac fibroblasts to differentiate into a myofibroblast phenotype. *J Biol Chem*. 2011;286:17365–17375. doi: 10.1074/jbc.M110.192682.
8. Neill T, Schaefer L, Iozzo RV. Decorin: a guardian from the matrix. *Am J Pathol*. 2012;181:380–387. doi: 10.1016/j.ajpath.2012.04.029.
9. Yin X, Cuello F, Mayr U, Hao Z, Hornshaw M, Ehler E, Avkiran M, Mayr M. Proteomics analysis of the cardiac myofilament subproteome reveals dynamic alterations in phosphatase subunit distribution. *Mol Cell Proteomics*. 2010;9:497–509. doi: 10.1074/mcp.M900275-MCP200.
10. Yin X, Bern M, Xing Q, Ho J, Viner R, Mayr M. Glycoproteomic analysis of the secretome of human endothelial cells. *Mol Cell Proteomics*. 2013;12:956–978. doi: 10.1074/mcp.M112.024018.
11. Guiraud S, van Wittenberghe L, Georger C, Scherman D, Kichler A. Identification of decorin derived peptides with a zinc dependent anti-myostatin activity. *Neuromuscul Disord*. 2012;22:1057–1068. doi: 10.1016/j.nmd.2012.07.002.
12. Stegemann C, Didangelos A, Barallobre-Barreiro J, Langley SR, Mandal K, Jahangiri M, Mayr M. Proteomic identification of matrix metalloproteinase substrates in the human vasculature. *Circ Cardiovasc Genet*. 2013;6:106–117. doi: 10.1161/CIRCGENETICS.112.964452.
13. Scott PG, McEwan PA, Dodd CM, Bergmann EM, Bishop PN, Bella J. Crystal structure of the dimeric protein core of decorin, the archetypal small leucine-rich repeat proteoglycan. *Proc Natl Acad Sci USA*. 2004;101:15633–15638. doi: 10.1073/pnas.0402976101.
14. Daquinag AC, Zhang Y, Amaya-Manzanares F, Simmons PJ, Kolonin MG. An isoform of decorin is a resistin receptor on the surface of adipose progenitor cells. *Cell Stem Cell*. 2011;9:74–86. doi: 10.1016/j.stem.2011.05.017.
15. Husberg C, Agnetti G, Holewinski RJ, Christensen G, Van Eyk JE. Dephosphorylation of cardiac proteins *in vitro* - a matter of phosphatase specificity. *Proteomics*. 2012;12:973–978. doi: 10.1002/pmic.201100116.
16. Charles RL, Burgoyne JR, Mayr M, Weldon SM, Hubner N, Dong H, Morisseau C, Hammock BD, Landar A, Eaton P. Redox regulation of soluble epoxide hydrolase by 15-deoxy-delta-prostaglandin J2 controls coronary hypoxic vasodilation. *Circ Res*. 2011;108:324–334. doi: 10.1161/CIRCRESAHA.110.235879.
17. Ungar D. Golgi linked protein glycosylation and associated diseases. *Semin Cell Dev Biol*. 2009;20:762–769. doi: 10.1016/j.semcdb.2009.03.004.
18. Parker BL, Palmisano G, Edwards AV, White MY, Engholm-Keller K, Lee A, Scott NE, Kolarich D, Hambly BD, Packer NH, Larsen MR, Cordwell SJ. Quantitative N-linked glycoproteomics of myocardial ischemia and reperfusion injury reveals early remodeling in the extracellular environment. *Mol Cell Proteomics*. 2011;10:M110.006833. doi: 10.1074/mcp.M110.006833.
19. Chen S, Birk DE. The regulatory roles of small leucine-rich proteoglycans in extracellular matrix assembly. *FEBS J*. 2013;280:2120–2137. doi: 10.1111/febs.12136.
20. Fisher LW, Termine JD, Young MF. Deduced protein sequence of bone small proteoglycan I (biglycan) shows homology with proteoglycan II (decorin) and several nonconnective tissue proteins in a variety of species. *J Biol Chem*. 1989;264:4571–4576.
21. Bianco P, Fisher LW, Young MF, Termine JD, Robey PG. Expression and localization of the two small proteoglycans biglycan and decorin in developing human skeletal and non-skeletal tissues. *J Histochem Cytochem*. 1990;38:1549–1563.
22. Iozzo RV, Schaefer L. Proteoglycans in health and disease: novel regulatory signaling mechanisms evoked by the small leucine-rich proteoglycans. *FEBS J*. 2010;277:3864–3875. doi: 10.1111/j.1742-4658.2010.07797.x.
23. Tocchi A, Parks WC. Functional interactions between matrix metalloproteinases and glycosaminoglycans. *FEBS J*. 2013;280:2332–2341. doi: 10.1111/febs.12198.
24. Vial C, Gutiérrez J, Santander C, Cabrera D, Brandan E. Decorin interacts with connective tissue growth factor (CTGF)/CCN2 by LRR12 inhibiting its biological activity. *J Biol Chem*. 2011;286:24242–24252. doi: 10.1074/jbc.M110.189365.

25. Bredrup C, Knappskog PM, Majewski J, Rødahl E, Boman H. Congenital stromal dystrophy of the cornea caused by a mutation in the decorin gene. *Invest Ophthalmol Vis Sci*. 2005;46:420–426. doi: 10.1167/iovs.04-0804.
26. Yang VW, LaBrenz SR, Rosenberg LC, McQuillan D, Höök M. Decorin is a Zn2+ metalloprotein. *J Biol Chem*. 1999;274:12454–12460.
27. Miura T, Kishioka Y, Wakamatsu J, Hattori A, Hennebry A, Berry CJ, Sharma M, Kambadur R, Nishimura T. Decorin binds myostatin and modulates its activity to muscle cells. *Biochem Biophys Res Commun*. 2006;340:675–680. doi: 10.1016/j.bbrc.2005.12.060.
28. Morissette MR, Cook SA, Foo S, McKoy G, Ashida N, Novikov M, Scherrer-Crosbie M, Li L, Matsui T, Brooks G, Rosenzweig A. Myostatin regulates cardiomyocyte growth through modulation of Akt signaling. *Circ Res*. 2006;99:15–24. doi: 10.1161/01.RES.0000231290.45676.d4.
29. Jiang MS, Liang LF, Wang S, Ratovitski T, Holmstrom J, Barker C, Stotish R. Characterization and identification of the inhibitory domain of GDF-8 propeptide. *Biochem Biophys Res Commun*. 2004;315:525–531. doi: 10.1016/j.bbrc.2004.01.085.
30. Breitbart A, Auger-Messier M, Molkentin JD, Heineke J. Myostatin from the heart: local and systemic actions in cardiac failure and muscle wasting. *Am J Physiol Heart Circ Physiol*. 2011;300:H1973–H1982. doi: 10.1152/ajpheart.00200.2011.
31. Biesemann N, Mendler L, Wietelmann A, Hermann S, Schäfers M, Krüger M, Boettger T, Borchardt T, Braun T. Myostatin regulates energy homeostasis in the heart and prevents heart failure. *Circ Res*. 2014;115:296–310. doi: 10.1161/CIRCRESAHA.115.304185.
32. Hardie DG, Ross FA, Hawley SA. AMPK: a nutrient and energy sensor that maintains energy homeostasis. *Nat Rev Mol Cell Biol*. 2012;13:251–262. doi: 10.1038/nrm3311.
33. Cantó C, Gerhart-Hines Z, Feige JN, Lagouge M, Noriega L, Milne JC, Elliott PJ, Puigserver P, Auwerx J. AMPK regulates energy expenditure by modulating NAD+ metabolism and SIRT1 activity. *Nature*. 2009;458:1056–1060. doi: 10.1038/nature07813.
34. Ausma J, Wijffels M, Thoné F, Wouters L, Allessie M, Borgers M. Structural changes of atrial myocardium due to sustained atrial fibrillation in the goat. *Circulation*. 1997;96:3157–3163.
35. Lee SJ, McPherron AC. Regulation of myostatin activity and muscle growth. *Proc Natl Acad Sci USA*. 2001;98:9306–9311. doi: 10.1073/pnas.151270098.
36. Rosenberg MA, Das S, Pinzon PQ, Knight AC, Sosnovik DE, Ellinor PT, Rosenzweig A. A novel transgenic mouse model of cardiac hypertrophy and atrial fibrillation. *J Atr Fibrillation*. 2012;2:1–15.
37. Callis TE, Pandya K, Seok HY, Tang RH, Tatsuguchi M, Huang ZP, Chen JF, Deng Z, Gunn B, Shumate J, Willis MS, Selzman CH, Wang DZ. MicroRNA-208a is a regulator of cardiac hypertrophy and conduction in mice. *J Clin Invest*. 2009;119:2772–2786. doi: 10.1172/JCI36154.
38. Ikeda Y, Sato K, Pimentel DR, Sam F, Shaw RJ, Dyck JR, Walsh K. Cardiac-specific deletion of LKB1 leads to hypertrophy and dysfunction. *J Biol Chem*. 2009;284:35839–35849. doi: 10.1074/jbc.M109.057273.
39. Parker BL, Thaysen-Andersen M, Solis N, Scott NE, Larsen MR, Graham ME, Packer NH, Cordwell SJ. Site-specific glycan-peptide analysis for determination of N-glycoproteome heterogeneity. *J Proteome Res*. 2013;12:5791–5800. doi: 10.1021/pr400783j.
40. Eckhard U, Marino G, Butler GS, Overall CM. Positional proteomics in the era of the human proteome project on the doorstep of precision medicine. *Biochimie*. 2016;122:110–118. doi: 10.1016/j.biochi.2015.10.018.

Glycoproteomics Reveals Decorin Peptides With Anti-Myostatin Activity in Human Atrial Fibrillation

Javier Barallobre-Barreiro, Shashi K. Gupta, Anna Zoccarato, Rika Kitazume-Taneike, Marika Fava, Xiaoke Yin, Tessa Werner, Marc N. Hirt, Anna Zampetaki, Alessandro Viviano, Mei Chong, Marshall Bern, Antonios Kourliouros, Nieves Domenech, Peter Willeit, Ajay M. Shah, Marjan Jahangiri, Liliana Schaefer, Jens W. Fischer, Renato V. Iozzo, Rosa Viner, Thomas Thum, Joerg Heineke, Antoine Kichler, Kinya Otsu and Manuel Mayr

Circulation. 2016;134:817-832; originally published online August 24, 2016;
doi: 10.1161/CIRCULATIONAHA.115.016423
Circulation is published by the American Heart Association, 7272 Greenville Avenue, Dallas, TX 75231

Print ISSN: 0009-7322. Online ISSN: 1524-4539

SUPPLEMENTAL MATERIAL

GLYCOPROTEOMICS REVEALS DECORIN PEPTIDES WITH ANTI-MYOSTATIN ACTIVITY IN HUMAN ATRIAL FIBRILLATION

Javier Barallobre-Barreiro, PhD[1], Shashi K. Gupta, PhD[2], Anna Zoccaratto, PhD[1], Rika Kitazume-Taneike, MD[1], Marika Fava, MSc[1,3], Xiaoke Yin, PhD[1], Tessa Werner, MSc[4], Marc N Hirt, MD, PhD[4], Anna Zampetaki, PhD[1], Alessandro Viviano, MD[3], Mei Chong, PhD[1], Marshall Bern, PhD[5], Antonios Kourliouros, MD[3], Nieves Domenech, PhD[6], Peter Willeit, MD, PhD[1], Ajay M Shah, MD[1], Marjan Jahangiri, MD[3], Liliana Schaefer, PhD[7], Jens W. Fischer, MD[8], Renato V. Iozzo, MD[9], Rosa Viner, PhD[10], Thomas Thum, MD, PhD[2], Joerg Heineke, PhD[11], Antoine Kichler, PhD[12], Kinya Otsu, MD, PhD[1], Manuel Mayr, MD, PhD[1].

[1] King's British Heart Foundation Centre, King's College London, London, UK
[2] Institute for Molecular and Translational Therapeutic Strategies, MH-Hannover, Germany
[3] St George's Hospital, NHS Trust, London, UK
[4] University Medical Center Hamburg-Eppendorf, Hamburg, Germany
[5] Protein Metrics, San Carlos, USA
[6] Biobanco A Coruña, INIBIC-Complexo Hospitalario Universitario de A Coruña, Spain
[7] Klinikum der Goethe-Universität, Frankfurt am Main, Germany
[8] Institute for Pharmacology and Clinical Pharmacology, Heinrich-Heine-University, Düsseldorf, Germany
[9] Sidney Kimmel Medical College at Thomas Jefferson University, Philadelphia, USA
[10] Thermo Fisher Scientific, San Jose, USA
[11] Experimental Cardiology, Department of Cardiology and Angiology, MH-Hannover, Germany
[12] Laboratoire Vecteurs: Synthèse et Applications Thérapeutiques, UMR 7199 CNRS Université de Strasbourg, Illkirch, France

Address for correspondence:

Manuel Mayr, MD, PhD, King's British Heart Foundation Centre, King's College London, 125 Coldharbour Ln, London, SE5 9NU, UK. Phone: +44 (0) 20 7848 5446, Fax: +44 (0) 20 7848 5298, Email: manuel.mayr@kcl.ac.uk .

ONLINE METHODS

Human cardiac tissue. Myocardial tissue samples were immediately snap frozen and stored in liquid nitrogen. The following samples were obtained: Atrial samples (~125mm^3) from patients who maintained SR after surgery or developed postoperative AF (n=7 per group, Supplemental Table I and VII); LAA and RAA from the same patient undergoing elective first-time coronary artery bypass surgery with the use of cardiopulmonary bypass (n=5). All patients were in SR before surgery and had no history of atrial fibrillation or other arrhythmias, presence of permanent pacemaker, or receiving any antiarrhythmic medications. None of them developed postoperative AF; LAA from patients in permanent atrial fibrillation and respective controls (n=6 per group, Supplemental Table VI); Additional atrial samples from patients with AF (n=13) and postoperative AF (n=10) and SR-SR controls (n=14) were used for qPCR analysis; samples from human left ventricles (LV) were obtained from Biobanco A Coruña, Complexo Hospitalario Universitario de A Coruña (Spain) from non-failing hearts donated for valve transplantation (n=7) under approval from the Galician Ethics Committee for Research following guidelines of Spanish Royal Decrees 2070/1999 and 1301/2006, which regulate the obtainment of human tissues for clinical and research purposes.

Protein extraction. 30-40 mg of frozen myocardial tissue was placed in ice-cold phosphate-buffered saline (PBS) to remove plasma contaminants. A protease inhibitor cocktail (Sigma-Aldrich) was included according to the manufacturer's instructions to inhibit broad range protease activity, and 25 mM EDTA was included to ensure inhibition of metalloproteases. Tissue samples were diced into smaller pieces to enhance the initial removal of plasma contaminants and the effective extraction of extracellular proteins.[1,2] A total of five PBS washes were carried out. Then, the diced samples were incubated with 0.5 M NaCl, 10 mM Tris, pH 7.5 supplemented with protease inhibitors (Sigma-Aldrich) and 25 mM EDTA. The

volume of the buffer was adjusted to 10:1 (µl/mg) of the tissue weight, and the samples were mildly vortexed for 1 h at room temperature. Subsequently, tissue samples were incubated with 0.1% SDS (10:1 buffer volume to tissue weight) supplemented with protease inhibitor mixtures and 25 mM EDTA. The samples were mildly vortexed for 16 h at room temperature to achieve removal of cellular components, taking particular care to ensure a low vortexing speed to avoid mechanical disruption of the ECM. The SDS solution was then removed and stored frozen for later use. Finally, the samples were incubated in 4 M guanidine hydrochloride (GuHCl), 50 mM sodium acetate, pH 5.8 (5:1 buffer volume to tissue weight) supplemented with protease inhibitor mixtures and 25 mM EDTA. Incubation was performed for 72 h at room temperature and vortexed vigorously to enhance mechanical disruption of the ECM components. GuHCl destabilizes the ionic, disulfide-dependent protein conformations[3] in large aggregating proteoglycans (versican, aggrecan, etc), small proteoglycans (decorin, biglycan, etc), cell attachment matrix glycoproteins such as type VI collagen, fibronectins and laminins and basement membrane components (perlecan, type IV collagen, etc). The guanidine extracts were mixed with 100% ethanol (10:1 volume ratio) at -20 °C overnight to ensure removal of guanidine and protease inhibitors, which would interfere with the later enrichment and digestion steps. Proteins were precipitated with centrifugation (16,000 g for 1 h), and the pellets were dried and kept at -20 °C for later use.

Enrichment of cardiac ECM glycoproteins. GuHCl extracts from left-right matched atrial samples (n=5) were further enriched in ECM glycoproteins using a lectin binding based protocol. Lectins are highly specific sugar-binding proteins, which have been used over the past decades to achieve sugar and glycoprotein isolation. To effectively enrich our GuHCl extracts in ECM glycoproteins, we employed a combination of two resin-bound lectins; wheat germ agglutinin (WGA) and

concanavalin A (Con A). WGA is a 38 kDa heterodimeric lectin that exerts a protective role in wheat. It binds to N-acetyl-D-glucosamine (GlcNAc) and sialic acid, which are present in the chitin of insects and cell membranes of yeast and bacteria. In mammals, WGA binds to GlcNAc from ECM-rich tissues and sialic acids from mucous membranes. Con A is a homotetramer composed of 26.5 kDa units isolated from jack bean, and exerts protective effect via agglutination of animal and yeast cells upon recognition of surface carbohydrates. The four binding sites of the tetramer specifically recognise α-D-mannosyl and α-D-glucosyl residues of ramified carbohydrate structures. With regards to the heart, it is important to mention that Con A displays unspecific avidity for hydrophobic ligands such as certain domains of tropomyosin.[4,5] The binding of saccharides and hydrophobic ligands, however, are neither competitive nor interactive.[6] Highly denaturing buffers are not suitable for lectin-based glycoprotein isolation. The ionic strength of 4M GuHCl enhances the extraction of ECM proteins, but it would also denature ConA and WGA (data not shown). Additionally, the presence of chelating agents such as EDTA, that efficiently inactivate metalloproteases during protein extraction, would inhibit interaction of lectins with carbohydrates. After ethanol precipitation, 100ug of protein from GuHCl extracts were re-solubilised for 1 hour using ConA/WGA binding buffer (Thermo Scientific), plus additional 0.125% SDS to enhance protein solubilisation and 1:100 of a broad spectrum protease inhibitor (Sigma-Aldrich). The glycoprotein fraction (GP) and the non-binding flow-through (FT) were obtained using a 1:1 mix of the ConA and WGA-based glycoprotein isolation kits (Thermo Scientific) according to the instructions of the manufacturer. The GP and FT fractions were desalted using 2mL Zeba Spin Columns (Thermo Scientific) and speed-vacuum dried.

Protein deglycosylation and gel electrophoresis. Dried GuHCl (input), GP and FT extracts were resuspended in deglycosylation buffer (50mM sodium phosphate, pH 7.0) and incubated at 37°C in agitation for 48 hrs. The following deglycosylation

enzymes were used: Endo-α-N-Acetylgalactosaminidase, β1,4- Galactosidase, Glucosaminidase, N-Glycosidase F, Neuraminidase (all purchased from Merk-Millipore), Chondroitinase ABC and endo β1,4-Galactosidase (both from Sigma-Aldrich). All deglycosylated extracts and NaCl extracts were denatured at 95°C for 5 min in sample buffer (100 mM Tris, pH 6.8, 40% glycerol, 0.2% SDS, 2% beta-mercaptoethanol, and 0.02% bromphenol blue) and 20 µg of protein was run at 150V for approximately 100 min using precast NuPAGE 4-12% Bis Tris Gels (Life Technologies). Gels were fixed and silver stained using a published protocol.[7]

Proteomics analysis. The gel bands were excised across the entire lanes, leaving no empty gel pieces behind. According to the differences in sample complexity, gels from NaCl and GuHCl extracts were cut into 16 bands per lane; GP and FT fractions were cut into 9 bands per lane. Subsequently, all gel bands were subjected to in-gel digestion with trypsin using an Investigator ProGest (Genomic Solutions) robotic digestion system according to a previously described protocol.[1] Tryptic peptides were lyophilised, reconstituted with 0.05% formic acid and separated on a nanoflow LC system (Dionex UltiMate 3000). Peptides were eluted with a 40 min gradient (10–25%B in 35 min, 25–40%B in 5 min, 90%B in 10 min, and 2%B in 30 min where A is 2% ACN, 0.1% formic acid in HPLC H_2O and B is 90% ACN, 0.1% formic acid in HPLC H_2O). The column (Dionex PepMap C18, 25-cm length, 75-um internal diameter, 3-um particle size) was coupled to a nanospray source (Picoview). Spectra were collected from an Orbitrap mass analyzer (LTQ-Orbitrap XL, ThermoFisher Scientific) using full ion scan mode over the mass-to-charge (m/z) range 450–1600. MS/MS was performed on the top six ions in each MS scan using the data-dependent acquisition mode with dynamic exclusion enabled.[8] MS/MS peak lists were generated by extract_msn.exe and matched to a human database (UniProtKB/Swiss-Prot Release 14.6, 21,669 protein entries) using Mascot (version 2.3.01, Matrix Science). Carboxyamidomethylation of cysteine was chosen as a fixed

modification and oxidation of methionine, lysine and proline were chosen as variable modifications. Oxidation of proline and lysine are crucial as variable modifications due to the large amounts of collagen present within ECM-derived samples.[9] The mass tolerance was set at 20 ppm for the precursor ions and 1.0 amu for fragment ions. Two missed cleavages were allowed. Scaffold (version 4.1.1, Proteome Software Inc., Portland, OR) was used to calculate the spectral counts and to validate MS/MS-based peptide and protein identifications. Peptide identifications were accepted if they could be established at greater than 95.0% probability as specified by the Peptide Prophet algorithm. Protein identifications were accepted if they could be established at greater than 99.0% probability with at least two independent peptides. Selection of ECM proteins was based on the Gene Ontology database. A "no enzyme" search was performed to identify peptides derived from non-tryptic cleavages. The MS/MS datasets have been deposited in PRIDE (dataset identifier PXD004465), a public repository for MS data (http://www.ebi.ac.uk/ pride/).

Western blot. For immunoblotting, we followed standard protocols. Briefly, 10µg of protein extracts were loaded per lane, separated on 4-12% gradient gels (NuPage, Invitrogen) and transferred to nitrocellulose membranes. Antibodies against the following human proteins were purchased: fibulin-2 (Santa Cruz, sc-271263), lumican (Santa Cruz, sc-33785), biglycan (Abcam, ab-58562), vitronectin (Santa Cruz, sc-30979), mimecan (Santa Cruz, sc-374463), N-terminal decorin (Sigma-Aldrich, SAB2100540), C-terminal decorin (Sigma-Aldrich, SAB2100539) and decorin internal (Santa Cruz, sc-22753). For immunoblotting on lysates from mouse cardiac tissue and rat cardiac myocytes we used antibodies against the following proteins: biglycan (Abcam, ab49701), pan-AMPK (Upstate, 07-181), phospho-Thr_{172} AMPK (Cell Signaling, 2535), phospho-SMAD-2 (Cell Signaling, 3108P), pan-SMAD-2 (Cell Signaling, 5339P), glyceraldehyde 3-phosphate dehydrogenase (Cell Signaling, 2118S), and phospho-Thr_{172} AMPK (Kinasource, PB-140). HRP-labelled secondary

antibodies for rabbit (Dako, P0217), mouse (Dako, P0260), goat (Dako, P0449) and Sheep Light Chain Specific (Jackson Immunoresearch, 213-032-177) were used according to the source of the primary antibody. Immunoblots were quantified by densitometry using Image-J software.

Mass spectrometry-based identification of glycosylation sites. For the identification of the glycosylation sites, a direct strategy using alternating HCD and ETD (HCD-alt-ETD) or HCD-product dependent ETD (HCD-pd-ETD) fragmentation on an Orbitrap Elite MS was pursued.[10,11] Protein extracts (GuHCl) from left and right atria in sinus rhythm were pooled (n=5) and 50µg of proteins were enriched for glycoproteins as described above. Afterwards the glycoprotein-enriched fractions were digested with trypsin and tryptic peptides were labelled with TMT0 to increase their charge state. In parallel, 50µg of the same samples were precipitated, digested with trypsin and tryptic peptides were labelled with TMT0 prior to glycopeptide enrichment by ZIC-HILIC purification.[12,13] The 2 preparations (glycoprotein- and glycopeptide-enriched peptides) were directly analysed by using HCD-alt-ETD or HCD-pd-ETD fragmentation on an Orbitrap Elite MS as previously described.[10,13] A Thermo Scientific EASY- nLCTM nano-HPLC system and Michrom Magic C18 spray tip 15 cm x 75 µm i.d. column (Auburn, CA) were used. Gradient elution was performed from 4-30% ACN in 0.1% formic acid over 60 min at a flow rate of 300 nL/min. The samples were analyzed with a Thermo Scientific Orbitrap Elite hybrid mass spectrometer with ETD. The following MS and MS/MS settings were used: FT: MSn AGCTarget = 3e4; MS/MS = 1 µscans, 200 ms max ion time; MS = 300-1800 m/z, 60000 resolution at m/z 400, MS Target = 1e6; MS/MS = Top 10 Data Dependent acquisition HCD Product Dependent acquisition ion trap ETD using product (oxonium) ions at m/z 138.0554; 163.0812, 204.0864. Dynamic Exclusion = repeat count 1, Duration 30 sec, Exclusion duration 90 sec; HCD Parameters: Collision Energy = 35%; resolution 15000@400. MSn Target Ion Trap = 5e3, 2

μscans, ETD anion AGC target = 2e6, charge dependent ETD reaction time was used. Thermo Scientific Proteome Discoverer 1.3 software was used to search MS/MS spectra against the Swiss-Prot database using MascotTM 2.3v (Matrix Science, Ltd.) and to generate a smaller database of identified glycoproteins. A prototype of the GlycoMasterTM (Bioinformatics Solution, Waterloo, ON, Canada) software was used for intact glycopeptides analysis. To compare abundances of non-tryptic decorin peptides, full MS intensities (before MS2) of individual peptides were quantified using Pinpoint software (version 1.3, Thermo Scientific).

Search for protease targets and structural information. The amino acid sequence for human decorin was used as input to search for putative cleavage sites for proteases on the PROSPER (PROtease Specificity Prediction servER) web server at https://prosper.erc.monash.edu.au/. Structural information for bovine decorin was previously published[14] and used for illustrative representation of decorin cleavage sites using the molecular visualization software PyMOL v1.8. Prediction of natively disordered regions in decorin structure was based on previous publications and the database for structural homology Phyre2 (Protein Homology/analogY Recognition Engine V 2.0) available online at http://www.sbg.bio.ic.ac.uk/phyre2.

Peptide synthesis and myostatin. All peptides were synthesized as previously described[15] by GeneCust (Dudelange, Luxembourg) matching the corresponding mouse decorin sequences. The sequence of the full N-terminal peptide was "DEASGIIPYDPDNPLISMCPYRCQCHLRVVQCSDLGLDKVP". The sequence of the shorter decorin peptide mimicking the cleaved form detected in patients with AF was "DNPLISMCPYRCQCHLRVVQCSDLGLDKVP". Notably, amino acid sequences for human, rat and mouse myostatin are 100% identical. Recombinant myostatin was purchased from R&D Systems (Minneapolis, USA).

P(CAGA)12-luciferase reporter assay. HEK293 cells (ATCC) were transfected with the pGL3(CAGA)12 reporter plasmid and were plated 24 hrs later on 48-well plates. The cells were cultured in DMEM medium with 1% fetal calf serum and recombinant mouse myostatin was added at a final concentration of 2.5 nM ± the full N-terminal peptide or the cleaved N-terminal peptide at different concentrations. The concentration of myostatin used in our experiments within the range of serum concentrations measured in humans.[16] Before addition to the cells, myostatin and the full or cleaved N-terminal peptide were preincubated in culture medium for 30 min at 37°C in the presence of 15 μM $ZnCl_2$. Subsequently, the HEK293 cells were cultured for 24 hours and were then lysed and luciferase activity was assayed, as previously described.[17] The results were normalized for protein content per well, which was determined by the Micro BCATM Protein Assay Kit (Thermo Scientific) and were calculated for each sample as the ratio of the specific luciferase activity per μg protein. The normalized luciferase activity in control cells without myostatin or peptide treatment was set to 100%.

Cardiac myocyte extraction and cell size measurements. Neonatal rat ventricular cardiac myocytes were isolated from post-natal day 1-3 old Wistar rat pups using trypsin and DNAse I digestion. 70000–80000 neonatal rat cardiac myocytes were seeded in 48 well plates in MEM medium (+Pencillin+Streptomycin+BrDu+5%FBS). After 48 hrs, cells were treated with 10μM phenylephrine and 10μM isoproterenol in 1%FBS medium to induce hypertrophy. Decorin-derived peptides at the appropriate concentrations were preincubated with myostatin (2.5nM) for 30 min and added to the culture medium. After 72 hrs of treatment, cells were washed with PBS and fixed in 4% para-formaldehyde (in PBS) for 15 min. Cells were washed twice with PBS and permeabilized with 0.1% Triton-X- 100 in PBS for 10 min at 4°C. Epitope blocking was carried out using 5% donkey serum in PBS for 30 min. Cells were incubated overnight in alpha-actinin sarcomeric antibody (Sigma a7811) at 1:1000 dilution in

5% donkey serum. Last, cells were washed and treated with secondary antibody anti-mouse Alexa 594 (Invitrogen) and Dapi at 1:1000 dilution for 45 min followed by a PBS wash. Images were taken with 20X objective using Nikon-DS-Qi MC camera and cell size measurement was done using NIS element BR 3 software (Nikon).

AMPK phosphorylation experiments. Neonatal rat ventricular cardiac myocytes were isolated from 1 to 2-days old Sprague-Dawley rats (Charles River Laboratories) as previously described.[18] Cells were cultured in plating medium (DMEM High Glucose, MEM199, Horse serum, Non-Heat inactivated Fetal Bovine Serum, Non-essential amino acids, Glutamine, Pen/Strep) for 24 hours before switching to a serum-free medium containing DMEM High Glucose, MEM199, Glutamine, Pen/Strep. After 24 hours, mouse or human decorin-derived peptides (20μM) were preincubated with myostatin (2.5 nM) for 30 min at room temperature and added to the culture medium. After 2 hours cells were treated for 72 hours with phenylephrine (10 μM) and isoproterenol (10 μM). Cells were lysed in lysis buffer (150mM NaCl, 50 mM Tris pH 8.0, 1.0% NP-40, 0.1% SDS) supplemented with Protease Inhibitor Cocktail (Sigma) and phosphatase inhibitors (PhosSTOP, Roche). Protein concentration was measured using the BCA assay (Pierce, UK).

RNA isolation. Total RNA from tissue or cultured cells was prepared using the miRNeasy kit (Qiagen) as described previously.[19] In brief, cardiac tissue was lysed and homogenised with 700μl of QIAzol reagent. Following a brief incubation at ambient temperature, 140 μl of chloroform was added and the solution was mixed vigorously. The samples were then centrifuged at 12,000 rpm for 15 min at 4°C. The aqueous phase was carefully transferred to a new tube and 1.5 volumes of ethanol were added. The samples were applied directly to columns and washed according to the company's protocol. Total RNA was eluted in 25 μl of nuclease free H_2O. For gene expression studies, 1μg of RNA was reversed transcribed into cDNA using the High Capacity Reverse Transcriptase kit (Life Technologies). Quantitative

polymerase chain reaction (qPCR) using Taqman Assays was used to assess the gene expression levels. Beta-actin was used as a normalization control.

Nuclear Magnetic Resonance (NMR) spectroscopy. The extraction buffer consisted of methanol, chloroform and H_2O (ratio 1:1:1). Tissue pieces (around 75mg) were homogenized using an orbital homogenizer (Precellys) for 30s at 5000 rpm twice and followed by centrifugation 1500 rpm at 4°C for 45 minutes to remove the precipitates. The methanol/H_2O phase was collected and evaporated using a speed-vac dryer at 30°C. The dried extracts were reconstituted in a 100mM sodium monophosphate buffer (pH 7.0) containing 500µM TMSP (sodium 3-(trimethylsilyl)propionate-2,2,3,3-d4), 1.5 mM sodium azide, 0.5mM EDTA and 100% deuterium oxide. All volumes were adjusted to the tissue weight on each sample. A 700 MHz Bruker spectrometer equipped with a cryogenic probe was used for 1D $^{+}$H-NMR data acquisition. H_2O resonance was suppressed using H_2O pre-saturation. $^{+}$H-NMR spectra were acquired using 9.3 kHz spectral width and 32 K data points with acquisition time of 1.67 s, relaxation delay of 5 s and 128 scans. The resulting spectra were processed to 65536 data points and corrected for phasing and zero referencing using NMRLab.[20] Resonance assignments and quantification were made with reference to Chenomx NMR Suite 7.1(Chenomx, Edomonton, Canada).

Langendorff mouse heart perfusion. 10-12 week-old C57BL/6J male mice (~26 g body weight) were purchased from Harlan (Harlan, UK). Mice were kept with a 12 h light–dark cycle, controlled humidity and temperature (20– 22 °C), fed standard chow and water ad libitum. All experiments were approved by institutional ethical review committee and conform to the UK Home Office Guidance on the Operation of the Animals Scientific Procedures Act 1986 (HMSO).

Mice were administered terminal anesthesia via intra-peritoneal pentobarbitone injection (~160 mg/kg body weight). Hearts were rapidly excised, cannulated and

perfused in Langendorff system and perfused at 75 mmHg pressure maintained by a STH peristaltic pump controller feedback system (AD Instruments, Oxford, UK), at 37 °C with Krebs–Henseleit (KH) buffer continuously gassed with 95% O_2/5% CO_2 (pH 7.4) containing (in mM): NaCl 118.5, KCl 4.7, $MgSO_4 \cdot 7H_2O$ 1.2, $NaHCO_3$ 25, KH_2PO_4 1.2, $CaCl_2$ 1.4, glucose 11. Cardiac function was assessed using a fluid-filled cling-film balloon inserted into the left ventricle (LV), and connected via a rigid polyethylene line to a pressure transducer (DTX Plus TNF-R, Becton-Dickinson) and a PowerLab system (AD Instruments, Australia). Hearts were paced at 550 bpm using a DS2A Isolated Voltage Stimulator (Digitimer Ltd, UK). The volume in the intraventricular balloon was adjusted using a 1.0 ml syringe to achieve an initial LV diastolic pressure of ~12 mm Hg. Functional parameters were monitored using LabChart software v.5 (AD Instruments, Australia) throughout the experiment.

Hearts were stabilized for a minimum of 20 minutes with KH buffer. After stabilization, myostatin (2.5 nM) or myostatin with decorin peptide (2.5 nM and 2 μM, respectively) were perfused for 20 minutes to achieve preconditioning. Notably, myostatin and decorin peptides were pre-incubated for 30 minutes at 37 °C in the presence of 15 μM $ZnCl_2$ prior to perfusion. After this time, perfusion solution was switched to KH buffer containing 10 μM phenylephrine (PE). At the end of each experiment, hearts were immediately snap frozen in liquid nitrogen. For protein extraction, ~30 mg of left ventricular tissue were homogenized with 20μL/mg of lysis buffer (113mM NaCl, 25 mM Tris pH 8.0, 2mM EGTA, 5mM EDTA, 1% Triton X-100, 0.1% SDS) supplemented with Protease Inhibitor Cocktail (Sigma) and phosphatase inhibitors (PhosSTOP, Roche). Protein concentration for each sample was measured using BCA assay (Pierce, UK). Western blots were performed as described above using 25 μg of protein per lane.

Statistical analysis. The spectral counts are given as total spectra, after normalization to the total number of spectra. Unpaired t-tests for unequal variances

were applied for the comparison between SR-SR and SR-AF patients. Paired t-tests were used for the comparison of matched LAA and RAA samples taken from the same individual. The ion intensities are given as total intensities, after normalization to the total intensity of decorin, and un-paired t-tests for unequal variances were applied. Spearman's correlation coefficients (rho, ρ) with P values were reported for the correlation between luciferase activity and decorin, whereas Pearson's correlations (r) were calculated for gene expression values of decorin in all LAA. An un-paired t-test for unequal variances was applied to detect significant differences on cardiac myocyte size after the addition of decorin-derived peptides – all are calculated against the zero dose. All statistical analyses were performed using the statistical software SPSS (version 22.0.0.0, IBM Corporation).

ONLINE REFERENCES

1. Barallobre-Barreiro J, Didangelos A, Schoendube FA, Drozdov I, Yin X, Fernández-Caggiano M, Willeit P, Puntmann VO, Aldama-López G, Shah AM, Doménech N, Mayr M. Proteomics analysis of cardiac extracellular matrix remodeling in a porcine model of ischemia/reperfusion injury. *Circulation.* 2012;125:789-802.

2. Didangelos A, Yin X, Mandal K, Baumert M, Jahangiri M, Mayr M. Proteomics characterization of extracellular space components in the human aorta. *Mol Cell Proteomics.* 2010;9:2048-2062.

3. Sajdera SW, Hascall VC. Proteinpolysaccharide complex from bovine nasal cartilage. A comparison of low and high shear extraction procedures. *J Biol Chem*. 1969;244:77-87.

4. Kirwan JP, Hodges RS. Critical interactions in the stability control region of tropomyosin. *J Struct Biol.* 2010;170:294-306.

5. Owen JB, Di Domenico F, Sultana R, Perluigi M, Cini C, Pierce WM, Butterfield DA. Proteomics-determined differences in the concanavalin-A-fractionated proteome of hippocampus and inferior parietal lobule in subjects with Alzheimer's disease and mild cognitive impairment: implications for progression of AD. *J Proteome Res.* 2009;8:471-482.

6. Edelman GM, Wang JL. Binding and functional properties of concanavalin A and its derivatives. III. Interactions with indoleacetic acid and other hydrophobic ligands. *J Biol Chem*. 1978;253:3016-3022.

7. Didangelos A, Yin X, Mandal K, Saje A, Smith A, Xu Q, Jahangiri M, Mayr M. Extracellular matrix composition and remodeling in human abdominal aortic aneurysms: a proteomics approach. *Mol Cell Proteomics.* 2011;10:M111.008128.

8. Yin X, Cuello F, Mayr U, Hao Z, Hornshaw M, Ehler E, Avkiran M, Mayr M. Proteomics analysis of the cardiac myofilament subproteome reveals dynamic alterations in phosphatase subunit distribution. *Mol Cell Proteomics.* 2010;9:497-509.

9. Pokidysheva E, Zientek KD, Ishikawa Y, Mizuno K, Vranka JA, Montgomery NT, Keene DR, Kawaguchi T, Okuyama K, Bächinger HP. Posttranslational modifications in type I collagen from different tissues extracted from wild type and prolyl 3-hydroxylase 1 null mice. *J Biol Chem.* 2013;288:24742-24752.

10. Saba J, Dutta S, Hemenway E, Viner R. Increasing the productivity of glycopeptides analysis by using higher-energy collision dissociation-accurate mass-product-dependent electron transfer dissociation. *Int J Proteomics.* 2012;2012:560391.

11. Zhao P, Viner R, Teo CF, Boons GJ, Horn D, Wells L. Combining high-energy C-trap dissociation and electron transfer dissociation for protein O-GlcNAc modification site assignment. *J Proteome Res.* 2011;10:4088-4104.

12. Neue K, Mormann M, Peter-Katalinić J, Pohlentz G. Elucidation of glycoprotein structures by unspecific proteolysis and direct nanoESI mass spectrometric analysis of ZIC-HILIC-enriched glycopeptides. *J Proteome Res.* 2011;10:2248-2260.

13. Yin X, Bern M, Xing Q, Ho J, Viner R, Mayr M. Glycoproteomic analysis of the secretome of human endothelial cells. *Mol Cell Proteomics.* 2013;12:956-978.

14. Scott PG, McEwan PA, Dodd CM, Bergmann EM, Bishop PN, Bella J. Crystal structure of the dimeric protein core of decorin, the archetypal small leucine-rich repeat proteoglycan. *Proc Natl Acad Sci U S A.* 2004;101:15633-15638.

15. Guiraud S, van Wittenberghe L, Georger C, Scherman D, Kichler A. Identification of decorin derived peptides with a zinc dependent anti-myostatin activity. Neu*romuscul Disord.* 2012;22:1057-1068.

16. Breitbart A, Scharf GM, Duncker D, Widera C, Gottlieb J, Vogel A, Schmidt S, Brandes G, Heuft HG, Lichtinghagen R, Kempf T, Wollert KC, Bauersachs J, Heineke J. Highly specific detection of myostatin prodomain by an immunoradiometric sandwich assay in serum of healthy individuals and patients. *PLoS One*. 2013;8:e80454.

17. Heineke J, Auger-Messier M, Correll RN, Xu J, Benard MJ, Yuan W, Drexler H, Parise LV, Molkentin JD. CIB1 is a regulator of pathological cardiac hypertrophy. *Nat Med.* 2010;16:872-879.

18. Zhang M, Kho AL, Anilkumar N, Chibber R, Pagano PJ, Shah AM, Cave AC. Glycated proteins stimulate reactive oxygen species production in cardiac myocytes: involvement of Nox2 (gp91phox)-containing NADPH oxidase. *Circulation.* 2006;113:1235-1243.

19. Zampetaki A, Kiechl S, Drozdov I, Willeit P, Mayr U, Prokopi M, Mayr A, Weger S, Oberhollenzer F, Bonora E, Shah A, Willeit J, Mayr M. Plasma microRNA profiling reveals loss of endothelial miR-126 and other microRNAs in type 2 diabetes. *Circ Res.* 2010;107:810-817.

20. Ludwig C, Gunther U. MetaboLab: advanced NMR data processing and analysis for metabolomics. *BMC Bioinformatics.* 2011;12:366.

ONLINE FIGURE LEGENDS

Supplementary Figure I. **Efficiency of protein extraction and glycoprotein enrichment**. **A)** Atrial specimens (5 matched LAA and RAA) were subject to a 3-step extraction for ECM proteins followed by further enrichment for glycoproteins in the 4M guanidine (GuHCl) extracts (input) using lectins. Protein distribution on the gels is shown for the input, the flow-through fraction and the glycoprotein-enriched fraction. **B)** The bar graph depicts the percentage of identified spectra (mean±SD) for the most abundant glycoproteins in 0.5 M NaCl and the GuHCl extracts after sequential extraction (red and blue bars, respectively). The percentage of glycoproteins in both extracts is shown in the pie charts. **C)** The glycoprotein-enriched and non-bound flow-through fractions of the GuHCl extracts were analysed by proteomics and the relative contribution of proteins is shown before and after enrichment.

Supplementary Figure II. **Distribution of ECM proteins after enrichment. A)** Venn diagram for the ECM-related glycoproteins present in each fraction. Highly insoluble polymeric glycoproteins, such as glycosylated collagens and laminins, are only soluble in GuHCl and were not detected in the glycoprotein-enriched extracts. **B)** Relative abundance of ECM-related glycoproteins, non-glycosylated ECM proteins and intracellular proteins on the 3 analyzed extracts from 5 matched LAA and RAA. Bar charts represent mean±SD.

Supplementary Figure III. Confirmation of decorin glycosylation in the heart. Glycosaminoglycans were removed by using chondroitinase ABC and keratanase. Further addition of N-deglycosylases removed N-linked oligosaccharides and allowed identification of a 40KDa decorin core protein. MS/MS spectra are representative examples for the detection of decorin glycosylation at positions Asn211 and Asn262 using the HCD-alt-ETD and HCD-pd-ETD methods.

Supplementary Figure IV. **Decorin-biglycan fragmentation pattern in the heart. A)** Proportion of tryptic and non-tryptic cleavage sites for different ECM proteins. **B)** Human decorin and biglycan amino acid sequences were aligned using ClustalW and the cleavage sites found for these proteins are displayed. Despite high sequence homology, only 2 cleavage sites were found for biglycan. Notably, the majority of cleavage sites mapped non-conserved regions.

Supplementary Figure V. Gene expression. A) qPCR analysis for CTGF expression in atrial (LAA, n=14) and ventricular tissue (LV, n=7). ***, $p<0.001$. **B)** Cathepsin G and K are implicated in proteolytic cleavage at the C-terminus of decorin. **C)** qPCR analysis for cathepsin G and K expression in LAA (n=14) and LV (n=7). **, $p<0.01$. Bar charts represent mean±SD.

Supplementary Figure VI. **Atrial size and decorin in AF. A)** Atrial sizes were calculated using 2D echocardiography. No differences were observed for patients who developed postoperative AF. Patients with permanent AF (AF) displayed left atrial dilatation. Asterisk (*) denotes $p<0.05$ on an ANOVA test. **B)** qPCR analysis for decorin and CTGF expression (SR-SR=14, SR-AF=10, AF=13). **C)** Immunoblots for decorin in atrial appendages from patients in SR and patients with permanent AF (n=6 per group). Densitometries on the the right panel display the comparison of the results with three different decorin antibodies. *, denotes $p<0.05$ and **, $p<0.01$. **D)** Pearson correlation (r) for expression values of decorin in all LAA samples using qPCR primers for the regions corresponding to three different antibody recognition sites. Bar charts represent mean±SD.

Supplementary Figure VII. **Decorin in postoperative AF. A)** Lower decorin levels in SR-AF patients were detected by immunoblotting using antibodies recognizing decorin with and without deglycosylation (an antibody to an N-terminal epitope and internal epitope, respectively). **B)** The bar graphs (mean±SD) show the quantification

of selected immunoblots for decorin (DCN) by densitometry (n=7 per group). The closely-related proteoglycan biglycan (BGN) showed no differences in expression. Coomassie staining was used as a loading control. **, p<0.01; “DG” denotes deglycosylated; A.U., arbitrary units.

Supplementary Figure VIII. MS/MS spectra. A) Representative spectra derived from the most abundant cleavage sites observed for decorin (PGS2) in cardiac atria. Retention times (RT) for the non-tryptic C- and N-ragged peptides involving the site Phe330-Ser331 are provided to exclude in-source fragmentation. The same strategy was used for the site Ser49-Leu50. The RT of the tryptic and the non-tryptic peptide is shown for comparison. **B)** The peptide arising from the N-terminal cleavage site at Ser49-Leu50 (LGPVcPFR) was more abundant in AF patients than in SR patients (labelled in red and green, respectively, n=6 per group) in absolute as well as relative terms after adjusting for total decorin levels. Mean±SD. *p<0.05; **p<0.01.

Supplementary Figure IX. Representation of decorin structure. The exposure of cleavage sites in the surface of decorin is shown. The site labeled in red is important for generation of CTGF-binding fragments, whereas those labeled in orange would generate MSTN-binding fragments. Note the absence of glycosylations (blue) near these sites that could interfere with protein processing. Collagen binding could hinder accessibility to sites in the concave face. Notably, the N-terminal region of decorin (i.e. region surrounding Ser49-Leu50, highlighted with a red square in the bottom panel) constitutes a natively structurally disordered region.

Supplementary Figure X. Activity of decorin derived peptides. A) Peptides were synthesized for the region near the N-terminus of decorin including the cysteine loop hairpin region. This region is conserved between mouse and human. The full sequence of active myostatin (108 amino acids long) is 100% conserved in mouse, rat and human (right panel). **B)** A longer N-terminal peptide also repressed

downstream SMAD3 activated pathways. This effect was however less pronounced than that observed for the shorter peptide (Figure 5C), probably due to competition with additional binding partners other than myostatin as peptides and myostatin were not pre-incubated for these experiments. Bars are mean±SD of triplicate experiments. **C)** Kernel density plot for the distribution of cardiac myocyte size after incubation with myostatin alone or myostatin and 20μM of decorin peptide (see Figure 5E and 5F).

Supplementary Figure XI. Proton-NMR and AMPK phosphorylation. A) Additional representative $^{+}$H-NMR spectra for cardiac extracts from wild type (blue) and decorin null (orange) mice, covering the indicated chemical shift range. “ppm” denotes parts per million. **B)** AMPK phosphorylation levels were measured using two different antibodies against the phosphorylated Thr_{172} on AMPK (i.e. raised in rabbit and goat). Myostatin was pre-incubated alone or with decorin N-terminal peptides mimicking the human or mouse sequences before addition to cardiac myocytes for 2 hrs and stimulation with phenylephrine and isoproterenol for 72 hrs. AMPK phosphorylation changes between cells containing peptides and myostatin alone to those treated with myostatin only were normalised to total AMPK (pan-AMPK). **C)** Densitometry data for *in vitro* experiments (n=4 per condition). *, denotes $p<0.05$ in paired t-tests. **D)** Densitometry data for *ex vivo* experiments (n=3 mouse hearts per condition). Mean±SD; *, denotes $p<0.05$ and **, $p<0.01$ in unpaired t-tests.

Supplementary Figure XII. Decorin cleavage in human atria. Decorunt and a C-terminal truncated form of decorin had been previously described (blue). The C-terminal cleavage detected in the present study (Phe330-Ser331) removes the CTGF binding domain of decorin resulting in a loss of approximately 3kDa. The additional N-terminal cleavage site (Ser49-Leu50) observed in patients with persistent AF gives rise to a decorin peptide with anti-myostatin activity.

Supplemental Table I. Clinical characteristics of patients from whom left atrial appendages were obtained.

Patients (n)	14
Age	68.6±9.1
Gender (% male)	85.7
CABG (%)	92.8
DM	0.0
Hypertension (%)	50
Previous MI (%)	35.8
Statins (%)	85.7
β-blockers (%)	71.4
Antiarrhythmic (Amiodarone) (%)	50%
Bypass time (min)	73.5±20.3
X clamp time (min)	48.1±14.4
AF during hospital stay (%)	50%

CABG: coronary artery bypass grafting; DM: diabetes mellitus; MI: myocardial infarction; X clamp time: cross-clamp time. Amiodarone was administered postoperatively. Atrial appendages were taken at the time of surgery. Data presented are means ± SD or percentages.

Supplemental Table II. ECM and ECM-associated proteins in human atrial appendages (n=14)

Identified Proteins (74)	Uniprot name	Uniprot Acc Number	MW (KD)	Total spectra	Unique spectra	Unique peptides	Max % coverage
Agrin	AGRIN_HUMAN	O00468	217	174	84	84	5.8
Alpha-1-acid glycoprotein 1	A1AG1_HUMAN	P02763	24	12	8	8	11.0
Alpha-1B-glycoprotein	A1BG_HUMAN	P04217	54	43	27	27	13.0
Annexin A2	ANXA2_HUMAN	P07355	20	12	9	9	15.0
Apolipoprotein A-I	APOA1_HUMAN	P02647	31	126	74	72	32.0
Apolipoprotein A-IV	APOA4_HUMAN	P06727	45	14	9	8	20.0
Apolipoprotein C-III	APOC3_HUMAN	P02656	13	18	13	10	16.0
Apolipoprotein E	APOE_HUMAN	P02649	36	159	51	44	41.0
Asporin	ASPN_HUMAN	Q9BXN1	43	109	43	43	29.0
Basal cell adhesion molecule	BCAM_HUMAN	P50895	67	147	78	78	20.0
Beta-2-glycoprotein 1	APOH_HUMAN	P02749	38	313	107	87	40.0
Biglycan	PGS1_HUMAN	P21810	35	1189	223	167	57.0
Cadherin-2	CADH2_HUMAN	P19022	97	11	6	6	4.8
Cathepsin G	CATG_HUMAN	P08311	29	22	14	14	19.0
Chymase	CMA1_HUMAN	P23946	27	64	36	32	26.0
Clusterin	CLUS_HUMAN	P10909	52	347	63	63	30.0
Collagen alpha-1(I)	CO1A1_HUMAN	P02452	139	2178	472	412	46.0
Collagen alpha-1(II)	CO2A1_HUMAN	P02458	134	41	11	11	2.2
Collagen alpha-1(III)	CO3A1_HUMAN	P02461	139	478	160	148	22.0
Collagen alpha-1(IV)	CO4A1_HUMAN	P02462	161	13	8	8	1.5
Collagen alpha-1(V)	CO5A1_HUMAN	P20908	184	69	25	25	3.6
Collagen alpha-1(VI)	CO6A1_HUMAN	P12109	109	826	173	144	21.0
Collagen alpha-1(VIII)	CO8A1_HUMAN	P27658	73	3	2	2	4.8
Collagen alpha-1(XV)	COFA1_HUMAN	P39059	142	35	15	15	3.0
Collagen alpha-1(XVIII)	COIA1_HUMAN	P39060	178	59	22	22	3.3
Collagen alpha-1(XXVIII)	COSA1_HUMAN	Q2UY09	117	6	4	4	2.8
Collagen alpha-2(I)	CO1A2_HUMAN	P08123	129	1835	371	332	41.0
Collagen alpha-2(IV)	CO4A2_HUMAN	P08572	168	10	6	6	3.0
Collagen alpha-2(V)	CO5A2_HUMAN	P05997	145	120	52	52	6.7
Collagen alpha-2(VI)	CO6A2_HUMAN	P12110	109	342	80	80	11.0
Collagen alpha-3(V)	CO5A3_HUMAN	P25940	172	3	2	2	2.8
Collagen alpha-3(VI)	CO6A3_HUMAN	P12111	322	2773	556	473	21.0
Decorin	PGS2_HUMAN	P07585	40	1660	366	242	65.0
Dermatopontin	DERM_HUMAN	Q07507	24	170	77	58	32.0
Dystroglycan	DAG1_HUMAN	Q14118	97	120	64	47	6.1
Elastin	ELN_HUMAN	P15502	62	3	2	2	5.3
Extracellular superoxide dismutase	SODE_HUMAN	P08294	26	9	6	6	10.0
Fibromodulin	FMOD_HUMAN	Q06828	43	9	5	4	8.0
Fibronectin	FINC_HUMAN	P02751	263	1253	328	308	20.0
Galectin-1	LEG1_HUMAN	P09382	15	68	46	37	44.0
Galectin-3	LEG3_HUMAN	P17931	26	31	21	20	16.0
Galectin-3-binding protein	LG3BP_HUMAN	Q08380	65	34	14	14	8.5
Glypican-1	GPC1_HUMAN	P35052	67	5	3	3	5.5
Lactadherin short form	MFGM_HUMAN	Q08431	38	25	14	14	15.0
Laminin subunit alpha-2	LAMA2_HUMAN	P24043	344	82	34	34	3.3
Laminin subunit alpha-4	LAMA4_HUMAN	Q16363	203	17	9	9	3.1
Laminin subunit alpha-5	LAMA5_HUMAN	O15230	400	44	26	26	1.2
Laminin subunit beta-1	LAMB1_HUMAN	P07942	200	21	13	13	2.8
Laminin subunit beta-2	LAMB2_HUMAN	P55268	196	174	80	80	12.0
Laminin subunit gamma-1	LAMC1_HUMAN	P11047	178	158	71	67	7.6
Leukocyte elastase inhibitor	ILEU_HUMAN	P30740	43	4	2	2	5.5
Lumican	LUM_HUMAN	P51884	38	728	209	153	36.0
Mast cell carboxypeptidase A	CBPA3_HUMAN	P15088	49	19	5	5	5.5
Matrix Gla protein	MGP_HUMAN	P08493	12	14	8	8	23.0
Metalloproteinase inhibitor 3	TIMP3_HUMAN	P35625	24	9	5	5	16.0
Mimecan	MIME_HUMAN	P20774	34	852	222	166	50.0
Natriuretic peptide A	ANF_HUMAN	P01160	11	339	57	49	38.0
Neural cell adhesion molecule L1	L1CAM_HUMAN	P32004	140	19	9	9	2.3
Neutrophil defensin 1	DEF1_HUMAN	P59665	10	20	12	12	19.0
Nidogen-1	NID2_HUMAN	Q14112	136	839	215	198	16.0
Nidogen-2	NID2_HUMAN	Q14112	151	1162	370	282	21.0
Periostin	POSTN_HUMAN	Q15063	93	27	12	12	7.3
Perlecan	PGBM_HUMAN	P98160	469	2498	750	658	18.0
Prolargin	PRELP_HUMAN	P51888	44	1168	279	183	46.0
Secreted frizzled-related protein 1	SFRP1_HUMAN	Q8N474	35	6	5	5	10.0
Secreted phosphoprotein 24	SPP24_HUMAN	Q13103	24	21	9	9	12.0
Serum amyloid P-component	SAMP_HUMAN	P02743	25	837	108	91	30.0
Target of Nesh-SH3	TARSH_HUMAN	Q7Z7G0	119	187	86	80	11.0
Tenascin-X	TENX_HUMAN	P22105	464	630	278	263	12.0
Transforming growth factor-beta-induced protein ig-h3	BGH3_HUMAN	Q15582	75	22	14	14	5.9
Tryptase beta-2	TRYB2_HUMAN	P20231	31	10	7	7	9.9
Tubulointerstitial nephritis antigen-like	TINAL_HUMAN	Q9GZM7	52	381	104	92	23.0
Versican	CSPG2_HUMAN	P13611	265	753	151	129	6.0
Vitronectin	VTNC_HUMAN	P04004	54	592	99	78	21.0

Supplemental Table III. ECM and ECM-associated glycoproteins in human atria after glycoprotein enrichment

Identified Proteins (48)	Uniprot name	Uniprot Acc Number	MW (KD)	Total spectra	Unique spectra	Unique peptides	Max % coverage	Fold change (RAA vs LAA) n=5, each	p-value
Alpha-1-acid glycoprotein 1	A1AG1_HUMAN	P02763	24	152	65	42	24	0.79	0.948
Alpha-1-acid glycoprotein 2	A1AG2_HUMAN	P19652	24	6	6	6	13	1.44	0.515
Alpha-1B-glycoprotein	A1BG_HUMAN	P04217	54	130	47	45	18	0.95	0.795
Alpha-2-HS-glycoprotein	FETUA_HUMAN	P02765	39	3	3	3	6.5	1.02	0.374
Basal cell adhesion molecule	BCAM_HUMAN	P50895	67	184	78	76	21	0.46	**0.042**
Beta-2-glycoprotein 1	APOH_HUMAN	P02749	38	217	75	55	26	1.08	0.620
Cadherin-13	CAD13_HUMAN	P55290	78	314	78	67	11	1.26	0.150
Cadherin-2	CADH2_HUMAN	P19022	100	139	49	43	6.7	0.71	**0.010**
Cartilage intermediate layer protein 1	CILP1_HUMAN	O75339	133	5	3	3	3.3	2.00	0.186
Clusterin	CLUS_HUMAN	P10909	52	45	17	17	14	1.68	0.290
Collagen alpha-1(XVIII) chain	COIA1_HUMAN	P39060	178	9	6	6	2.7	1.01	0.374
Collagen alpha-3(VI) chain	CO6A3_HUMAN	P12111	344	15	11	11	1.2	2.79	0.358
Collagen alpha-6(VI) chain	CO6A6_HUMAN	A6NMZ7	247	7	5	4	1.6	1.06	0.364
Decorin	PGS2_HUMAN	P07585	40	24	14	12	14	2.87	0.367
Fibrillin-1	FBN1_HUMAN	P35555	312	1485	250	208	9	0.87	0.203
Fibronectin	FINC_HUMAN	P02751	263	510	155	146	15	1.10	0.661
Fibulin-2	FBLN2_HUMAN	P98095	127	693	130	104	16	1.82	**0.015**
Galectin-3-binding protein	LG3BP_HUMAN	Q08380	65	14	4	4	3.8	0.67	0.790
Hepatoma-derived growth factor	HDGF_HUMAN	P51858	26	53	35	32	45	1.23	0.475
Insulin-like growth factor-binding protein 7	IBP7_HUMAN	Q16270	29	4	3	3	19	1.02	0.374
Intercellular adhesion molecule 1	ICAM1_HUMAN	P05362	58	41	23	23	18	3.04	0.277
Kininogen-1	KNG1_HUMAN	P01042	72	33	21	21	8.9	1.94	0.358
Laminin subunit beta-2	LAMB2_HUMAN	P55268	196	170	53	49	4.8	0.72	0.518
Laminin subunit gamma-1	LAMC1_HUMAN	P11047	178	255	76	60	4.4	0.59	0.162
Latent-transforming growth factor beta-binding protein 2	LTBP2_HUMAN	Q14767	195	13	9	9	1.3	1.20	0.828
Latent-transforming growth factor beta-binding protein 4	LTBP4_HUMAN	Q8N2S1	173	22	14	14	3.6	9.34	**0.046**
Lumican	LUM_HUMAN	P51884	38	501	123	104	26	1.38	**0.039**
Matrix-remodeling-associated protein 7	MXRA7_HUMAN	P84157	21	12	8	8	14	0.78	0.730
Mimecan	MIME_HUMAN	P20774	34	84	46	45	18	1.50	0.059
Neural cell adhesion molecule 1	NCAM1_HUMAN	P13591	95	142	62	54	9.8	0.90	0.771
Neural cell adhesion molecule L1	L1CAM_HUMAN	P32004	140	10	6	6	2.5	1.14	0.075
Nidogen-1	NID1_HUMAN	P14543	136	50	28	28	4.1	0.95	0.894
Nidogen-2	NID2_HUMAN	Q14112	151	65	31	30	4.2	0.37	**0.003**
Perlecan	PGBM_HUMAN	P98160	469	22	10	10	0.91	1.52	0.557
Proactivator polypeptide	SAP_HUMAN	P07602	58	45	29	29	7.1	0.89	0.735
Prolargin	PRELP_HUMAN	P51888	44	39	19	18	20	0.90	0.910
Protein AMBP	AMBP_HUMAN	P02760	39	168	63	49	24	1.05	0.647
Proteoglycan 4	PRG4_HUMAN	Q92954	151	12	10	10	3.4	1.75	0.525
RPE-spondin	RPESP_HUMAN	Q8IVN8	30	3	2	2	8.7	0.98	0.374
Secreted phosphoprotein 24	SPP24_HUMAN	Q13103	24	2	2	2	10	1.01	0.374
Serum amyloid P-component	SAMP_HUMAN	P02743	25	164	40	40	26	1.14	0.436
Target of Nesh-SH3	TARSH_HUMAN	Q7Z7G0	119	242	75	72	13	1.39	0.172
Tenascin	TENA_HUMAN	P24821	241	42	16	14	5.1	9.40	0.269
Tenascin-X	TENX_HUMAN	P22105	464	1104	307	278	11	0.71	0.177
Tubulointerstitial nephritis antigen-like	TINAL_HUMAN	Q9GZM7	52	31	18	18	6.2	0.81	0.644
Versican core protein	CSPG2_HUMAN	P13611	373	550	132	99	3.5	1.03	0.787
Vitronectin	VTNC_HUMAN	P04004	54	24	14	14	4.6	2.72	**0.050**
Zinc-alpha-2-glycoprotein	ZA2G_HUMAN	P25311	34	25	20	20	19	1.12	0.811

Supplemental Table IV. N-linked and O-linked glycosylation sites in human atrial appendages

Protein Name	UniProt ID	Peptide	Glycosite position	Glycosite Status	Glycans (NHFAGNa)*	Observed m/z	z	Observed (M+H)	Calc. mass (M+H)	Off-by-x error	Mass error (ppm)	Score	Sample	Enrichment type	MS method
Apolipoprotein A-IV	APOA4_HUMAN	R.[+224.152]SLAP[+15.995]YAQDT[+203.079]QEK[+224.152].L	T230	novel	1 0 0 0 0 0	673.346	3	2018.024	2018.033	0	-4.3	111.9	RA	Glycoprotein	HCDaltETD
Apolipoprotein A-IV	APOA4_HUMAN	R.[+224.152]SLAP[+15.995]YAQDT[+203.079]QEK[+224.152].L	T230	novel	1 0 0 0 0 0	673.348	3	2018.030	2018.033	0	-1.5	113.0	RA	Glycoprotein	HCDaltETD
Beta-2-glycoprotein 1	APOH_HUMAN	K.[+224.152]LGN{+2204.772}{+21.982}WSAMPSC[+57.021]K[+224.152].	N253	known	4 5 0 2 0 1	982.161	4	3925.624	3925.625	0	-0.3	157.0	LA	Glycoprotein	HCDaltETD
Beta-2-glycoprotein 1	APOH_HUMAN	K.[+224.152]LGN{+2204.772}WSAMPSC[+57.021]K[+224.152].A	N253	known	4 5 0 2 0 0	976.917	4	3904.644	3903.643	1	-0.6	226.9	LA	Glycopeptide	HCDaltETD
Beta-2-glycoprotein 1	APOH_HUMAN	K.[+224.152]LGN{+2226.755}WSAMPSC[+57.021]K[+224.152].A	N253	known	4 5 0 2 0 1	982.413	4	3926.631	3925.625	1	0.7	230.3	LA	Glycoprotein	HCDaltETD
Beta-2-glycoprotein 1	APOH_HUMAN	R.[+224.152]VYK[+224.152]PSAGN{+2204.772}N[+0.984]SLYR.D	N162	known	4 5 0 2 0 0	1031.961	4	4124.821	4122.816	2	-0.5	236.8	RA	Glycopeptide	HCDaltETD
Beta-2-glycoprotein 1	APOH_HUMAN	R.[+224.152]VYK[+224.152]PSAGN{+2204.772}NSLYR.D	N162	known	4 5 0 2 0 0	1031.466	4	4122.842	4121.832	1	1.7	191.9	LA	Glycoprotein	HCDaltETD
Beta-2-glycoprotein 1	APOH_HUMAN	R.[+224.152]VYK[+224.152]PSAGN{+2204.772}NSLYR.D	N162	known	4 5 0 2 0 0	1031.714	4	4123.834	4121.832	2	-1.2	196.8	LA	Glycoprotein	HCDaltETD
Beta-2-glycoprotein 1	APOH_HUMAN	R.[+224.152]VYK[+224.152]PSAGN{+2204.772}NSLYR.D	N162	known	4 5 0 2 0 0	1031.212	4	4121.827	4121.832	0	-1.2	232.9	LA	Glycoprotein	HCDaltETD
Beta-2-glycoprotein 1	APOH_HUMAN	R.[+224.152]VYK[+224.152]PSAGN{+2204.772}NSLYR.D	N162	known	4 5 0 2 0 0	1031.465	4	4122.837	4121.832	1	0.5	276.6	LA	Glycoprotein	HCDaltETD
Beta-2-glycoprotein 1	APOH_HUMAN	R.[+224.152]VYK[+224.152]PSAGN{+2204.772}NSLYR.D	N162	known	4 5 0 2 0 0	1031.712	4	4123.827	4121.832	2	-2.7	272.5	LA	Glycoprotein	HCDaltETD
Beta-2-glycoprotein 1	APOH_HUMAN	R.[+224.152]VYK[+224.152]PSAGN{+2204.772}NSLYR.D	N162	known	4 5 0 2 0 0	1031.213	4	4121.829	4121.832	0	-0.7	240.9	LA	Glycoprotein	HCDaltETD
Beta-2-glycoprotein 1	APOH_HUMAN	R.[+224.152]VYK[+224.152]PSAGN{+2204.772}NSLYR.D	N162	known	4 5 0 2 0 0	1031.463	4	4122.830	4121.832	1	-1.2	263.3	LA	Glycoprotein	HCDaltETD
Beta-2-glycoprotein 1	APOH_HUMAN	R.[+224.152]VYK[+224.152]PSAGN{+2204.772}NSLYR.D	N162	known	4 5 0 2 0 0	1031.212	4	4121.827	4121.832	0	-1.2	301.6	RA	Glycopeptide	HCDaltETD
Beta-2-glycoprotein 1	APOH_HUMAN	R.[+224.152]VYK[+224.152]PSAGN{+2229.634}NSLYR.D	N162	known	3 10 0 0 0 0	1037.461	4	4146.822	4146.826	0	-0.9	146.8	LA	Glycoprotein	HCDpdETD
Beta-2-glycoprotein 1	APOH_HUMAN	R.[+224.152]VYK[+224.152]PSAGN{+2350.830}NSLYR.D	N162	known	4 5 1 2 0 0	1067.979	4	4268.896	4267.890	1	0.6	209.0	LA	Glycoprotein	HCDaltETD
Beta-2-glycoprotein 1	APOH_HUMAN	R.[+224.152]VYK[+224.152]PSAGN{+2375.824}NSLYR.D	N162	known	3 10 1 0 0 0	1073.976	4	4292.882	4292.884	0	-0.5	234.0	RA	Glycoprotein	HCDpdETD
Beta-2-glycoprotein 1	APOH_HUMAN	R.[+224.152]VYKPSAGN{+2204.772}{+21.982}NSLYR.D	N162	known	4 5 0 2 0 1	980.920	4	3920.658	3919.661	1	-1.6	271.6	RA	Glycopeptide	HCDpdETD
Beta-2-glycoprotein 1	APOH_HUMAN	R.[+224.152]VYKPSAGN{+2204.772}N[+0.984]SLYR.D	N162	known	4 5 0 2 0 0	975.673	4	3899.668	3898.663	1	0.5	285.6	RA	Glycopeptide	HCDaltETD
Beta-2-glycoprotein 1	APOH_HUMAN	R.[+224.152]VYKPSAGN{+2204.772}NSLYR.D	N162	known	4 5 0 2 0 0	975.176	4	3897.683	3897.679	0	1.0	297.4	RA	Glycopeptide	HCDaltETD
Basal cell adhesion molecule	BCAM_HUMAN	F.[+224.152]LTDRS[+656.228]GARPR.L	S72	novel	1 1 0 1 0 0	670.341	3	2009.009	2009.003	0	2.7	241.1	RA	Glycoprotein	HCDaltETD
Basal cell adhesion molecule	BCAM_HUMAN	F.[+224.152]LTDRS[+656.228]GARPR.L	S72	novel	1 1 0 1 0 0	670.340	3	2009.005	2009.003	0	1.0	245.0	RA	Glycoprotein	HCDaltETD
Basal cell adhesion molecule	BCAM_HUMAN	F.[+224.152]LTDRS[+678.210]GARPR.L	S72	novel	1 1 0 1 0 1	677.669	3	2030.993	2030.985	0	3.9	185.5	RA	Glycoprotein	HCDaltETD
Cadherin-2	CADH2_HUMAN	I.[+224.152]IT[+678.210]VAAGLDR.E	T332	novel	1 1 0 1 0 1	606.639	3	1817.903	1817.888	0	8.4	259.5	RA	Glycoprotein	HCDaltETD
Neural cell adhesion molecule L1-like protein	CHL1_HUMAN	N.[+224.152]ILRFS[+365.132]GQR.N	S871	novel	1 1 0 0 0 0	522.626	3	1565.862	1565.853	0	5.5	195.0	RA	Glycoprotein	HCDaltETD
Clusterin	CLUS_HUMAN	R.[+224.152]K[+224.152][+15.995]TLLS[+365.132]NLEEAK[+224.152].K	S72	novel	1 1 0 0 0 0	767.104	3	2299.297	2299.289	0	3.4	153.8	LA	Glycoprotein	HCDaltETD
Clusterin	CLUS_HUMAN	R.[+224.152]K[+224.152][+15.995]TLLS[+365.132]NLEEAK[+224.152].K	S72	novel	1 1 0 0 0 0	767.105	3	2299.300	2299.289	0	4.5	226.7	RA	Glycoprotein	HCDaltETD
Clusterin	CLUS_HUMAN	R.[+224.152]LAN{+2204.772}LTQGEDQYYLR.V	N374	known	4 5 0 2 0 0	1029.195	4	4113.757	4112.759	1	-1.3	254.9	LA	Glycoprotein	HCDaltETD
Clusterin	CLUS_HUMAN	R.[+224.152]LAN{+2204.772}LTQGEDQYYLR.V	N374	known	4 5 0 2 0 0	1028.945	4	4112.759	4112.759	0	0.1	188.8	LA	Glycoprotein	HCDaltETD
Clusterin	CLUS_HUMAN	R.EIRHN{+2256.851}STGC[+57.021]LR.M	N291	known	8 3 1 0 0 0	900.634	4	3599.516	3599.516	0	-0.1	174.0	LA	Glycoprotein	HCDpdETD
Collagen alpha-2(I)	CO1A2_HUMAN	R.[+224.152]GDQGP[+15.995]VGRT[+568.212]GEVG.A	T831	novel	2 1 0 0 0 0	679.994	3	2037.967	2036.951	1	6.3	219.9	LA	Glycopeptide	HCDaltETD
Collagen alpha-2(I)	CO1A2_HUMAN	R.[+224.152]GDQGP[+15.995]VGRT[+568.212]GEVG.A	T831	novel	2 1 0 0 0 0	679.659	3	2036.962	2036.951	0	5.8	226.1	LA	Glycopeptide	HCDaltETD
Collagen alpha-2(I)	CO1A2_HUMAN	R.[+224.152]GDQGP[+15.995]VGRT[+568.212]GEVG.A	T831	novel	2 1 0 0 0 0	679.658	3	2036.961	2036.951	0	5.0	187.9	RA	Glycopeptide	HCDaltETD
Collagen alpha-1(IV)	CO4A1_HUMAN	K.[+224.152]GSIGIPGMPGS[+511.190]PGLK[+224.152].G	S1095	novel	1 1 1 0 0 0	776.749	3	2328.232	2327.230	1	-0.6	148.8	LA	Glycoprotein	HCDaltETD
Collagen alpha-1(IV)	CO4A1_HUMAN	R.[+224.152]HSQTIDDPQC[+57.021]PSGT[+203.079]K[+224.152].I	T1464	novel	1 0 0 0 0 0	774.715	3	2322.131	2322.128	0	1.3	148.6	LA	Glycoprotein	HCDaltETD
Collagen alpha-2(IV)	CO4A2_HUMAN	R.[+224.152]GLHGLP[+15.995]GT[+203.079]K[+224.152].G	T1204	novel	1 0 0 0 0 0	516.300	3	1546.884	1546.884	0	0.3	143.5	RA	Glycopeptide	HCDaltETD
Collagen alpha-1(VI)	CO6A1_HUMAN	R.IALVIT[+365.132]DGRSDTQR.D	T732	novel	1 1 0 0 0 0	478.247	4	1909.964	1909.971	0	-3.7	165.4	LA	Glycoprotein	HCDaltETD
Collagen alpha-2(VI)	CO6A2_HUMAN	K.PQQVRN{+2215.825}MTLFSDLVAEK[+224.152].F	N785	known	7 4 1 0 0 0	1104.760	4	4416.016	4416.004	0	2.7	207.4	RA	Glycopeptide	HCDaltETD
Collagen alpha-3(VI)	CO6A3_HUMAN	E.[+224.152]RVT[+969.305]QLTR.E	T1206	novel	1 1 0 2 0 1	689.670	3	2066.994	2066.984	0	4.8	199.2	RA	Glycopeptide	HCDpdETD
Collagen alpha-6(VI)	CO6A6_HUMAN	R.[+224.152]AEFN[+406.159]LTTYRSK[+224.152][+15.995].R	N2034	novel	2 0 0 0 0 0	734.056	3	2200.152	2200.138	0	6.4	160.9	LA	Glycopeptide	HCDaltETD
Cartilage oligomeric matrix protein	COMP_HUMAN	K.[+224.152]S[+203.079]S[+365.132]TGPGEQLR.N	S642, S643	novel	1 0 0 0 0 0, 1 1 0 0 0 0	608.636	3	1823.893	1823.876	0	9.2	161.5	LA	Glycopeptide	HCDaltETD
Collagen alpha-1(XXVIII)	COSA1_HUMAN	K.[+224.152]GPK[+224.152]S[+511.190]NLLAR.K	S31	novel	1 1 1 0 0 0	639.026	3	1915.064	1915.063	0	0.4	174.4	LA	Glycopeptide	HCDaltETD
Versican core protein	CSPG2_HUMAN	K.[+224.152]HLVT[+947.323]TVPKDPEAAEAR.R	T1419	novel	1 1 0 2 0 0	727.359	4	2906.413	2905.394	1	5.6	224.0	LA	Glycopeptide	HCDpdETD
Versican core protein	CSPG2_HUMAN	K.[+224.152]HLVTT[+947.323]VPKDPEAAEAR.R	T1419	novel	1 1 0 2 0 0	727.106	4	2905.401	2905.394	0	2.5	279.8	RA	Glycopeptide	HCDpdETD
Versican core protein	CSPG2_HUMAN	K.[+224.152]NTIIDIDHT[+203.079]K[+224.152].P	T2583	novel	1 0 0 0 0 0	456.007	4	1821.007	1821.000	0	3.8	210.2	LA	Glycoprotein	HCDaltETD
Dystroglycan	DAG1_HUMAN	K.[+224.152]P[+15.995]TVT[+365.132]IR.T	T369	known	1 1 0 0 0 0	431.238	3	1291.699	1291.699	0	-0.2	244.1	RA	Glycopeptide	HCDaltETD
Dystroglycan	DAG1_HUMAN	P.RVT[+656.228]TK[+224.152]VSITR.L	T463	novel	1 1 0 1 0 0	681.031	3	2041.080	2041.091	0	-5.5	243.1	LA	Glycopeptide	HCDaltETD
Dystroglycan	DAG1_HUMAN	P.RVT[+656.228]TK[+224.152]VSITR.L	T463	novel	1 1 0 1 0 0	681.032	3	2041.080	2041.091	0	-5.5	235.0	RA	Glycopeptide	HCDpdETD
EMILIN-1	EMIL1_HUMAN	R.[+224.152]LSRLEDRFN[+0.984]S[+947.323]T.L	S415	known	1 1 0 2 0 0	837.383	3	2510.135	2510.140	0	-2.3	128.7	LA	Glycoprotein	HCDaltETD
Fibulin-2	FBLN2_HUMAN	R.[+224.152]STGPEGVT[+947.323]HAPSLGK[+224.152].A	T357	novel	1 1 0 2 0 0	945.793	3	2835.363	2833.361	2	-1.7	202.1	LA	Glycoprotein	HCDaltETD
Fibulin-2	FBLN2_HUMAN	R.[+224.152]STGPEGVT[+947.323]HAPSLGK[+224.152].A	T357	novel	1 1 0 2 0 0	945.128	3	2833.369	2833.361	0	2.6	253.2	LA	Glycoprotein	HCDaltETD
Fibulin-2	FBLN2_HUMAN	R.[+224.152]STGPEGVT[+947.323]HAPSLGK[+224.152].A	T357	novel	1 1 0 2 0 0	945.124	3	2833.357	2833.361	0	-1.4	234.9	LA	Glycoprotein	HCDpdETD

Fibulin-2	FBLN2_HUMAN	R.[+224.152]STGPEGVTHAPS[+969.305]LGK[+224.152].A	S361	novel	1 1 0 2 0 1	952.787	3	2856.346	2855.343	1	-0.1	208.3	LA	Glycoprotein	HCDaltETD
Fibrillin-1	FBN1_HUMAN	K.[+224.152]LC[+57.021]S[+511.190]VPMVIPGR.P	S390	novel	1 1 1 0 0 0	655.334	3	1963.987	1963.997	0	-5.0	145.8	LA	Glycoprotein	HCDaltETD
Alpha-2-HS-glycoprotein	FETUA_HUMAN	K.[+224.152]AALAAFNAQNN{+2204.772}GSNFQLEEISR.A	N176	known	4 5 0 2 0 0	1199.780	4	4796.097	4794.078	2	2.5	243.7	LA	Glycoprotein	HCDaltETD
Alpha-2-HS-glycoprotein	FETUA_HUMAN	K.[+224.152]VC[+57.021]QDC[+57.021]PLLAPLN{+2204.772}DTR.V	N156	known	4 5 0 2 0 0	1051.449	4	4202.774	4200.772	2	-1.1	220.1	LA	Glycoprotein	HCDaltETD
Alpha-2-HS-glycoprotein	FETUA_HUMAN	K.[+224.152]VC[+57.021]QDC[+57.021]PLLAPLN{+2204.772}DTR.V	N156	known	4 5 0 2 0 0	1050.946	4	4200.762	4200.772	0	-2.2	192.0	LA	Glycoprotein	HCDaltETD
Laminin subunit beta-2	LAMB2_HUMAN	L.[+224.152]S[+365.132]ISDR.L	S460	novel	1 1 0 0 0 0	389.532	3	1166.580	1166.579	0	1.3	262.0	LA	Glycoprotein	HCDaltETD
Lumican	LUM_HUMAN	D.[+224.152]LQLT[+656.228]HNK[+224.152][+15.995].I	T145	novel	1 1 0 1 0 0	658.680	3	1974.025	1974.017	0	4.4	229.0	RA	Glycoprotein	HCDaltETD
Lumican	LUM_HUMAN	K.[+224.152]K[+224.152]LHINHNN{+2352.846}LTESVGPLPK[+224.152].S	N127	potential	6 7 0 0 0 0	1008.085	5	5036.395	5036.412	0	-3.4	186.8	LA	Glycoprotein	HCDaltETD
Lumican	LUM_HUMAN	K.[+224.152]LHINHNN{+2081.717}LTESVGPLPK[+224.152].S	N127	potential	4 5 1 1 0 1	1104.514	4	4415.033	4413.035	2	-1.9	175.7	RA	Glycoprotein	HCDpdETD
Lumican	LUM_HUMAN	K.LHINHNN{+2350.830}LTESVGPLPK.S	N127	potential	4 5 1 2 0 0	1059.215	4	4233.839	4233.844	0	-1.2	112.7	RA	Glycopeptide	HCDpdETD
Mimecan	MIME_HUMAN	K.[+224.152]DEAIT[+947.323]PLPPK[+224.152].K	T80	known	1 1 0 2 0 0	826.081	3	2476.228	2476.222	0	2.6	156.0	LA	Glycoprotein	HCDaltETD
Mimecan	MIME_HUMAN	K.[+224.152]DEAIT[+969.305]PLPPK[+224.152].K	T80	known	1 1 0 2 0 1	833.405	3	2498.201	2498.203	0	-1.1	134.9	LA	Glycoprotein	HCDaltETD
Mimecan	MIME_HUMAN	K.[+224.152]DEAIT[+969.305]PLPPK[+224.152].K	T80	known	1 1 0 2 0 1	833.739	3	2499.201	2498.203	1	-2.3	185.7	LA	Glycoprotein	HCDaltETD
Nidogen-1	NID1_HUMAN	D.[+224.152]LATT[+365.132]RLGLEDVGTTPFSYK[+224.152]ALR.R	T301	novel	1 1 0 0 0 0	645.355	5	3222.744	3222.751	0	-2.0	194.5	LA	Glycoprotein	HCDaltETD
Decorin	PGS2_HUMAN	K.[+224.152]GLNNLAK[+224.152][+15.995]LGLSFNSISAVDN{+1054.370}GSLANTPHLRELHLDNNK[+224.152].L	N262	known	2 4 0 0 0 0	967.672	6	5800.994	5799.944	1	8.1	294.5	LA	Glycoprotein	HCDaltETD
Decorin	PGS2_HUMAN	L.[+224.152]SFNSISAVDN{+2083.747}GSLANTPHLR.E	N262	known	5 3 0 1 0 0	1102.990	4	4408.938	4407.946	1	-2.4	147.5	RA	Glycoprotein	HCDpdETD
Decorin	PGS2_HUMAN	N.[+224.152]SISAVDN{+1809.666}GSLANTPHLR.E	N262	known	5 4 1 0 0 0	947.187	4	3785.725	3785.722	0	0.8	272.6	LA	Glycopeptide	HCDaltETD
Decorin	PGS2_HUMAN	N.[+224.152]SISAVDN{+1809.666}GSLANTPHLR.E	N262	known	5 4 1 0 0 0	947.186	4	3785.721	3785.722	0	-0.4	286.4	RA	Glycopeptide	HCDaltETD
Decorin	PGS2_HUMAN	N.[+224.152]SISAVDN{+1809.666}GSLANTPHLR.E	N262	known	5 4 1 0 0 0	947.434	4	3786.715	3785.722	1	-2.7	220.3	RA	Glycopeptide	HCDaltETD
Decorin	PGS2_HUMAN	N.[+224.152]SISAVDN{+2100.762}GSLANTPHLR.E	N262	known	5 4 1 0 1 0	1019.958	4	4076.810	4076.817	0	-1.9	202.7	RA	Glycopeptide	HCDaltETD
Decorin	PGS2_HUMAN	N.[+224.152]SISAVDN{+2350.830}GSLANTPHLR.E	N262	known	4 5 1 2 0 0	1082.978	4	4328.891	4326.886	2	-0.5	196.1	RA	Glycopeptide	HCDaltETD
Decorin	PGS2_HUMAN	R.[+224.152]IADTN{+1257.449}ITSIPQGLPPSLTELHLDGNK[+224.152].I	N211	known	3 4 0 0 0 0	1113.557	4	4451.208	4450.201	1	0.8	157.6	RA	Glycoprotein	HCDpdETD
Decorin	PGS2_HUMAN	R.[+224.152]IADTN{+1622.582}ITSIPQ[+0.984]GLPPSLTELHLDGNK[+224.1	N211	known	4 5 0 0 0 0	1205.340	4	4818.338	4816.317	2	3.0	199.3	RA	Glycoprotein	HCDpdETD
Podocan	PODN_HUMAN	L.[+224.152]NLQNN[+0.984]RLT[+365.132]SR.G	T133	novel	1 1 0 0 0 0	452.238	4	1805.928	1805.924	0	2.4	249.7	LA	Glycopeptide	HCDaltETD
Prolargin	PRELP_HUMAN	R.[+224.152]LEHLYLN[+0.984]N{+2059.735}{+21.982}NSIEK[+224.152].I	N320	potential	4 5 1 1 0 1	1030.204	4	4117.795	4117.823	0	-6.9	164.5	RA	Glycopeptide	HCDaltETD
Proteoglycan 4	PRG4_HUMAN	K.[+224.152]ET[+365.132]TTTNK.Q	T289	novel	1 1 0 0 0 0	461.893	3	1383.664	1383.674	0	-6.8	181.6	RA	Glycopeptide	HCDaltETD
Serum amyloid P-component	SAMP_HUMAN	R.[+224.152]ESVTDHVNLITPLEK[+224.152]PLQN{+2204.772}FTLC[+57.021	N51	known	4 5 0 2 0 0	1125.928	5	5625.610	5624.612	1	-0.9	193.3	RA	Glycoprotein	HCDaltETD
Serum amyloid P-component	SAMP_HUMAN	R.[+224.152]ESVTDHVNLITPLEKPLQN{+2449.899}FTLC[+57.021]FR.A	N51	known	6 4 2 1 0 0	1129.933	5	5645.638	5645.586	0	9.2	335.8	RA	Glycoprotein	HCDaltETD
Tenascin-X	TENX_HUMAN	L.[+224.152]RLGQM[+15.995]T[+203.079]VR.D	T2273	novel	1 0 0 0 0 0	468.593	3	1403.765	1403.768	0	-2.1	263.3	LA	Glycoprotein	HCDaltETD
Vitronectin	VTNC_HUMAN	K.[+224.152]N{+1710.598}GSLFAFR.G	N169	known	3 5 0 1 0 0	949.412	3	2846.221	2846.224	0	-0.9	108.4	LA	Glycopeptide	HCDaltETD

Supplemental Table V. Cardiac ECM and ECM-associated proteins with non-tryptic peptides identified by proteomics

Protein name	Protein accession number	MW (kDa)	Total identified spectra	Total non-tryptic spectra	Samples with non-tryptic spectra	Unique non-tryptic spectra	Total non-tryptic sites
Fibronectin	FINC_HUMAN	263	1824	16	5	3	3
Perlecan	PGBM_HUMAN	469	1715	1	1	1	1
Decorin	**PGS2_HUMAN**	**40**	**1657**	**198**	**9**	**22**	**18**
Collagen alpha-1(I) chain	CO1A1_HUMAN	139	1073	4	3	1	2
Collagen alpha-1(III) chain	CO3A1_HUMAN	139	731	2	2	2	4
Laminin subunit gamma-1	LAMC1_HUMAN	178	686	2	2	1	1
Prolargin	PRELP_HUMAN	44	635	1	1	1	1
Collagen alpha-2(I) chain	CO1A2_HUMAN	129	619	4	2	1	1
Lumican	LUM_HUMAN	38	596	46	7	8	7
Fibrillin-1	FBN1_HUMAN	312	516	49	7	3	3
Nidogen-1	NID1_HUMAN	136	452	1	1	1	1
Beta-2-glycoprotein 1	APOH_HUMAN	38	322	4	2	1	1
Biglycan	PGS1_HUMAN	42	319	4	3	2	2
Serum amyloid P-component	SAMP_HUMAN	25	277	3	3	1	1
Collagen alpha-3(VI) chain	CO6A3_HUMAN	344	271	2	2	1	1
Mimecan	MIME_HUMAN	34	175	5	4	4	4
Target of Nesh-SH3	TARSH_HUMAN	119	166	25	7	2	2
Cadherin-13	CAD13_HUMAN	78	130	4	1	2	2
Dermatopontin	DERM_HUMAN	24	127	30	3	9	8
EMILIN-1	EMIL1_HUMAN	107	49	5	4	1	1
Cadherin-2	CADH2_HUMAN	100	44	1	1	1	1
Dystroglycan	DAG1_HUMAN	97	21	5	3	1	1
Collagen alpha-2(V) chain	CO5A2_HUMAN	145	9	9	3	2	2
Tenascin	TENA_HUMAN	241	8	2	1	1	1
TOTAL		**-**	**12422**	**423**	**-**	**72**	**69**

Supplemental Table VI. Clinical characteristics of patients in SR and persistent AF.

	Persistent AF cohort	
	SR (n=6)	AF (n=6)
Age	63.6±5.5	71.2±5.4
Gender (% male)	100.0	100.0
CABG (%)	100.0	100.0
DM	33.3	16.7
Hypertension (%)	50.0	66.7
Previous MI (%)	16.6	50.0
Statins (%)	83.3	66.7
β-blockers (%)	66.6	50.0
Bypass time (min)	63±11.8	94.0±8.7*
X clamp time (min)	44.4±7.6	57.8±7.2
AF during hospital stay (%)	0.0	100.0*
Days to AF	N/A	N/A

CABG: coronary artery bypass grafting; DM: diabetes mellitus; MI: myocardial infarction; X clamp time: cross-clamp time; N/A not applicable. Data presented are means ± SD or percentages. P-values for comparisons between patient groups were derived from *t* tests; p values for categorical variables were derived from Fisher's exact test. Significant differences ($p<0.05$) are labeled with an asterisk (*).

Supplemental Table VII. Clinical characteristics of patients in SR who developed AF postoperatively (SR-AF) or maintained SR throughout (SR-SR).

	Post-operative AF cohort	
	SR-SR (n=7)	**SR-AF (n=7)**
Age	64.7±9.3	72.5±7.4
Gender (% male)	85.7	85.7
CABG (%)	100.0	85.7
DM	0.0	0.0
Hypertension (%)	28.6	71.4
Previous MI (%)	28.6	42.9
Statins (%)	85.7	85.7
β-blockers (%)	71.4	71.4
Antiarrhythmic (Amiodarone) (%)	0.0	100.0* (postop.)
Bypass time (min)	74.1±22.5	72.3±19.7
X clamp time (min)	45.71±13.3	50.4±16.2
AF during hospital stay (%)	0.0	100.0*
Days to AF	N/A	2.8±1.3

CABG: coronary artery bypass grafting; DM: diabetes mellitus; MI: myocardial infarction; X clamp time: cross-clamp time; N/A not applicable. Amiodarone was administered postoperatively. Atrial appenadges were taken at the time of surgery. Data presented are means ± SD or percentages. P-values for comparisons between patient groups were derived from *t* tests; p values for categorical variables were derived from Fisher's exact test. Significant differences ($p<0.05$) are labeled with an asterisk (*).

Supplementary Figure I

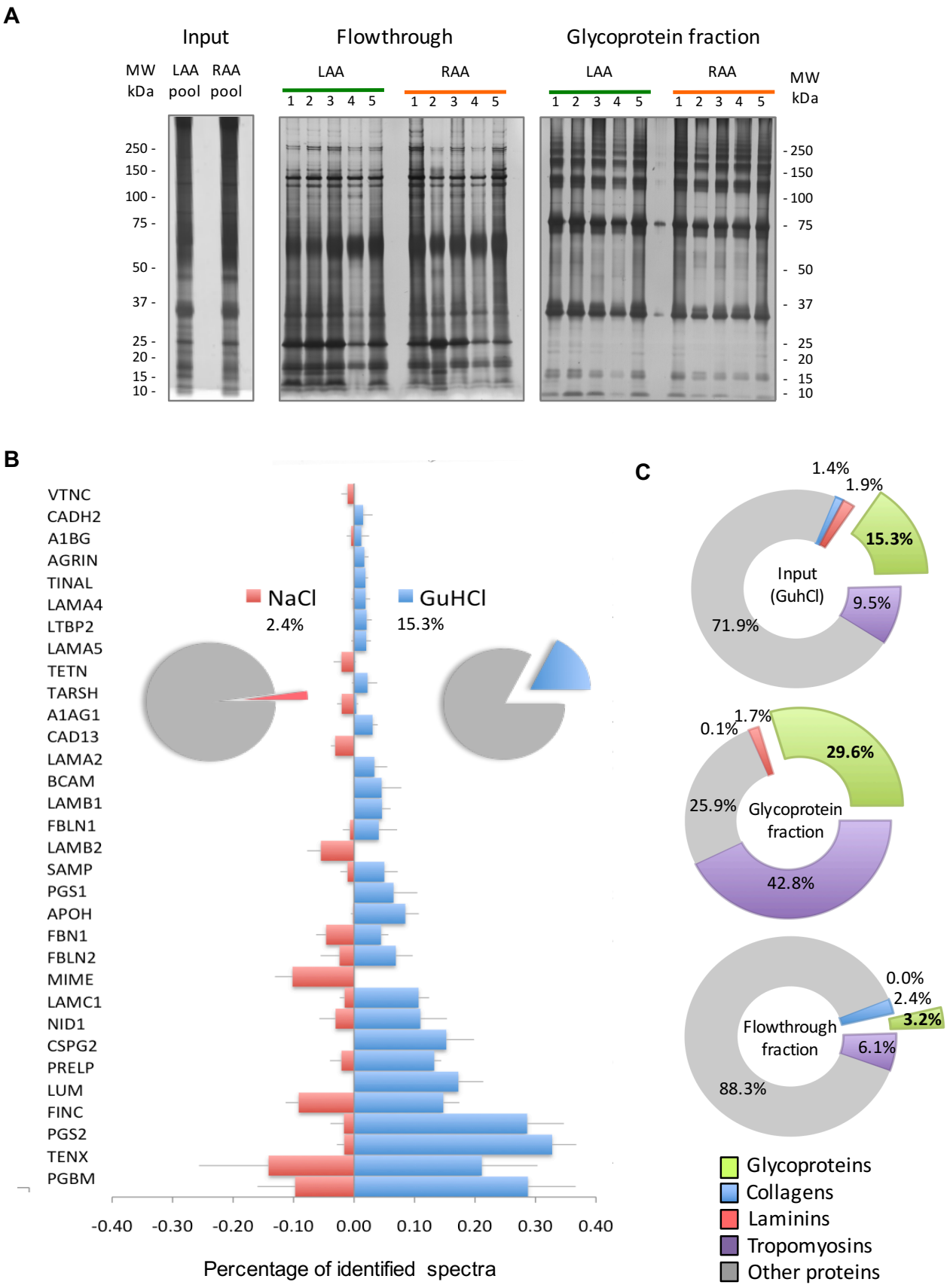

Supplementary Figure II

A

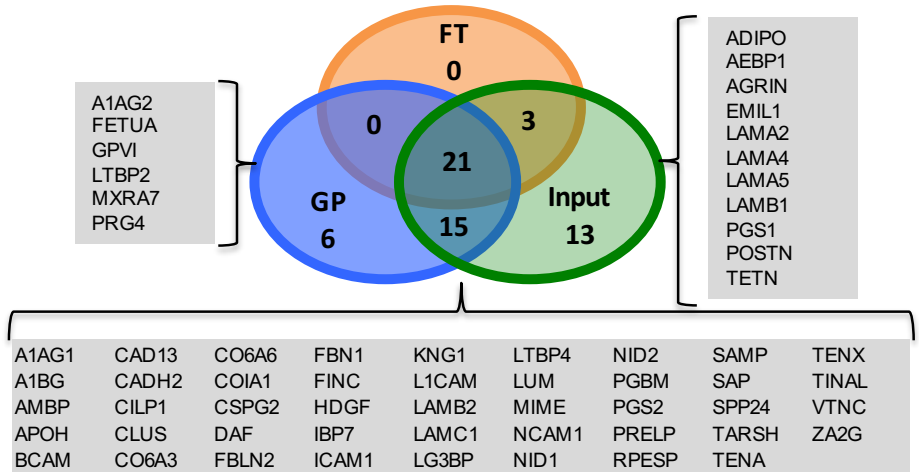

B

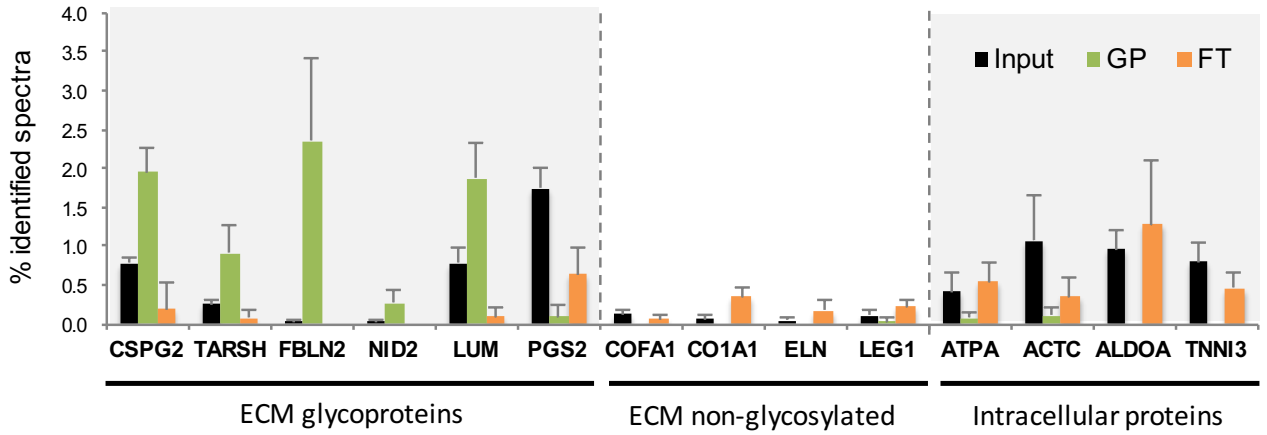

Supplementary Figure III

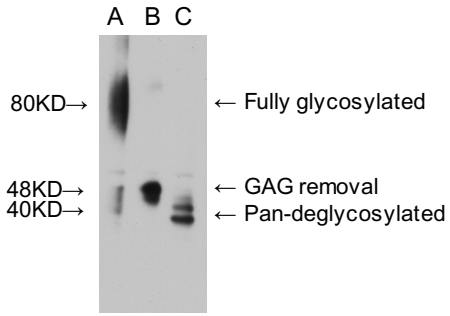

Decorin (PGS2_HUMAN) glycosite: **Asn211**

I^{TMT}ADTN(HexNac$_4$Hex$_5$)ITSIPdQGLPPSLTELHLDGNK^{TMT}

Method: **HCD product-dependent ETD**

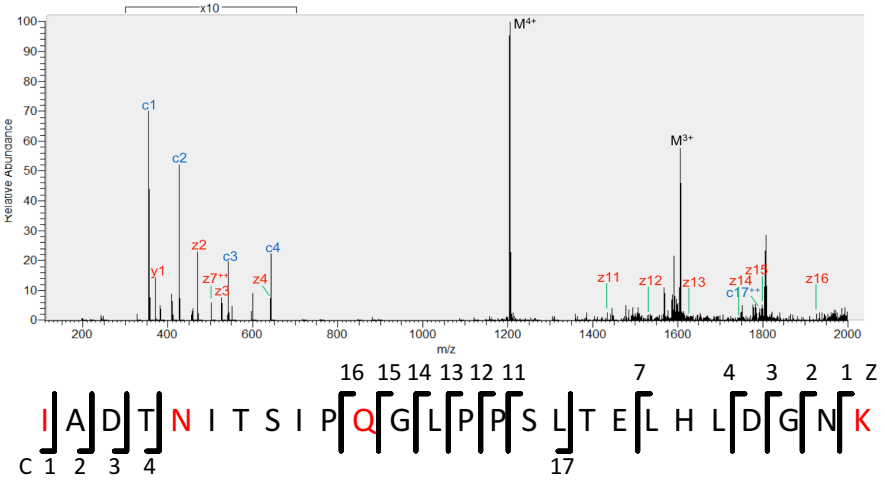

Decorin (PGS2_HUMAN) glycosite: **Asn262**

N.^{TMT}SISAVDN(HexNac$_5$Hex$_4$Fuc$_1$)GSLANTPHLR.E

Method: **Alternating HCD-ETD**

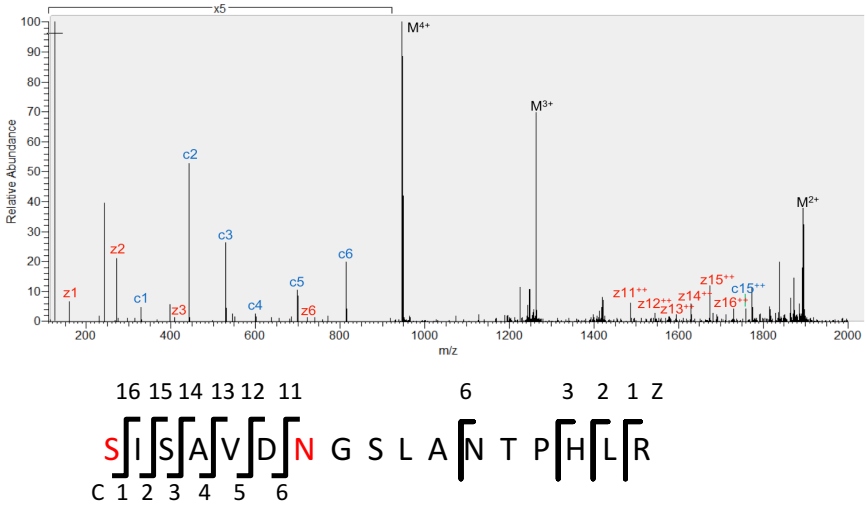

Decorin (PGS2_HUMAN) glycosite: **Asn262**

L.S^{TMT}FNSISAVDN(HexNac$_5$Hex$_3$SA$_1$)GSLANTPHLR.E

Method: **HCD product-dependent ETD**

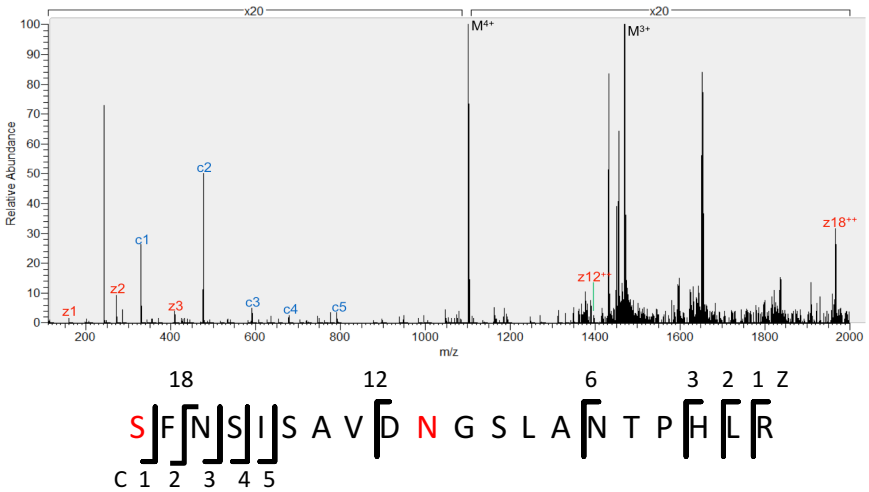

Supplementary Figure IV

A

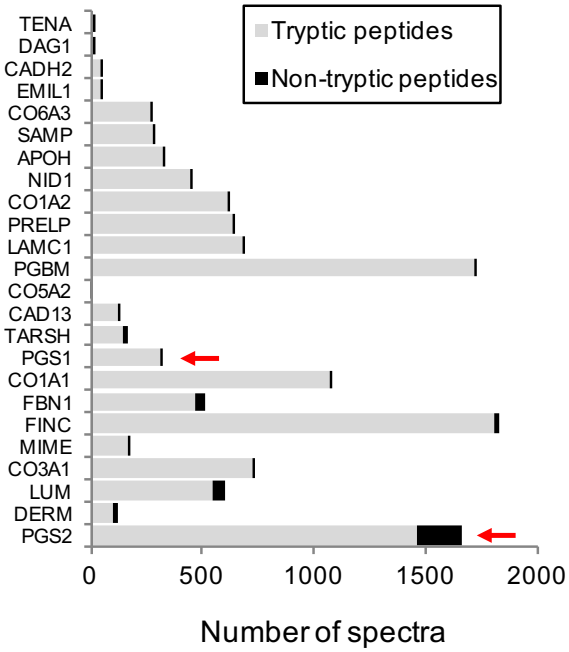

B

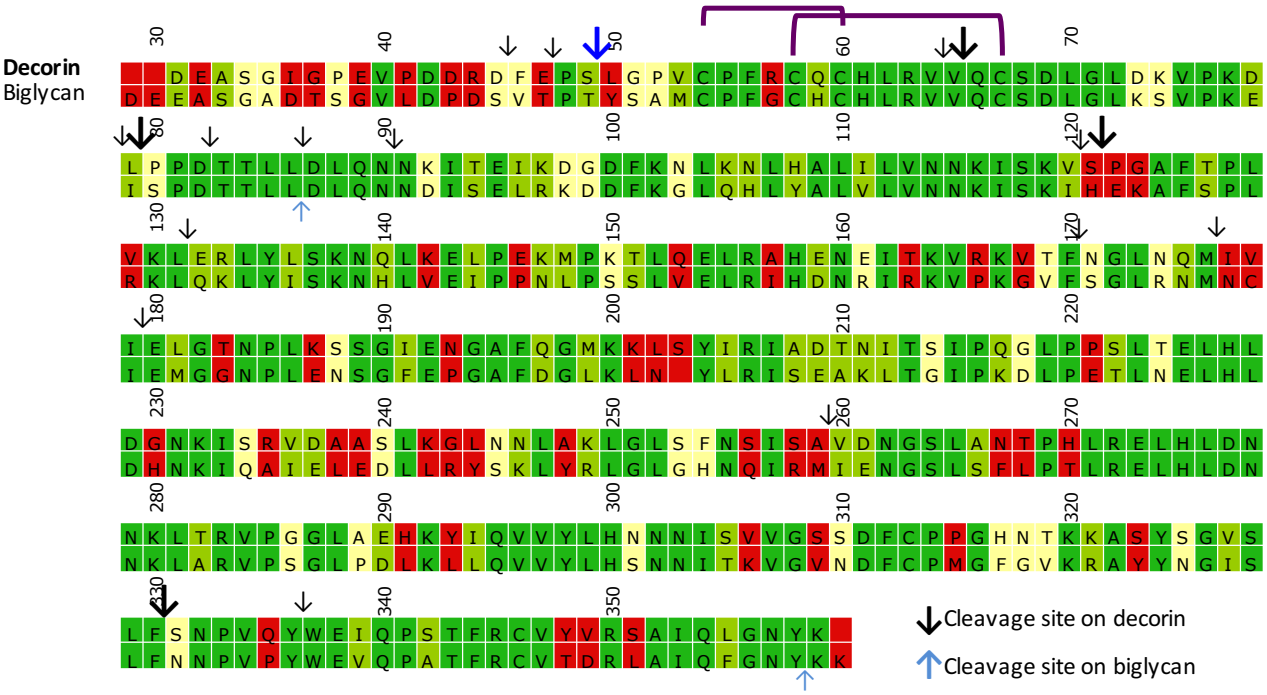

Supplementary Figure V

A

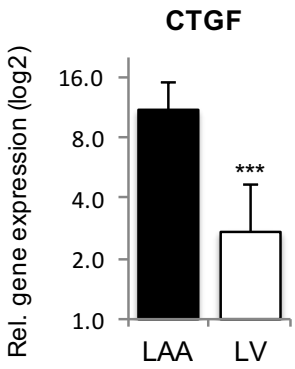

B

Input: Decorin, human	Segment	Nfragment	Cfragment	Score
Cathepsin G (S01.133)	VSLFISNPV	38.94 kDa	3.54 kDa	1.34
Cathepsin K (C01.036)	VSLFISNPV	38.94 kDa	3.54 kDa	1.06

C

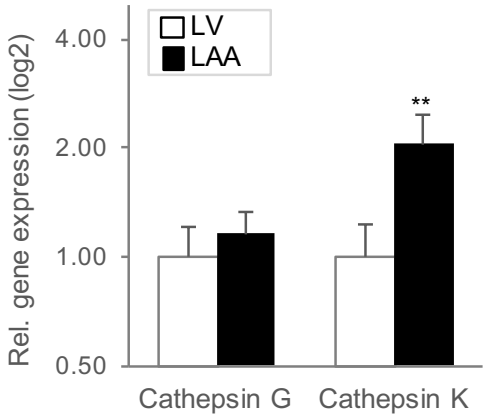

Supplementary Figure VI

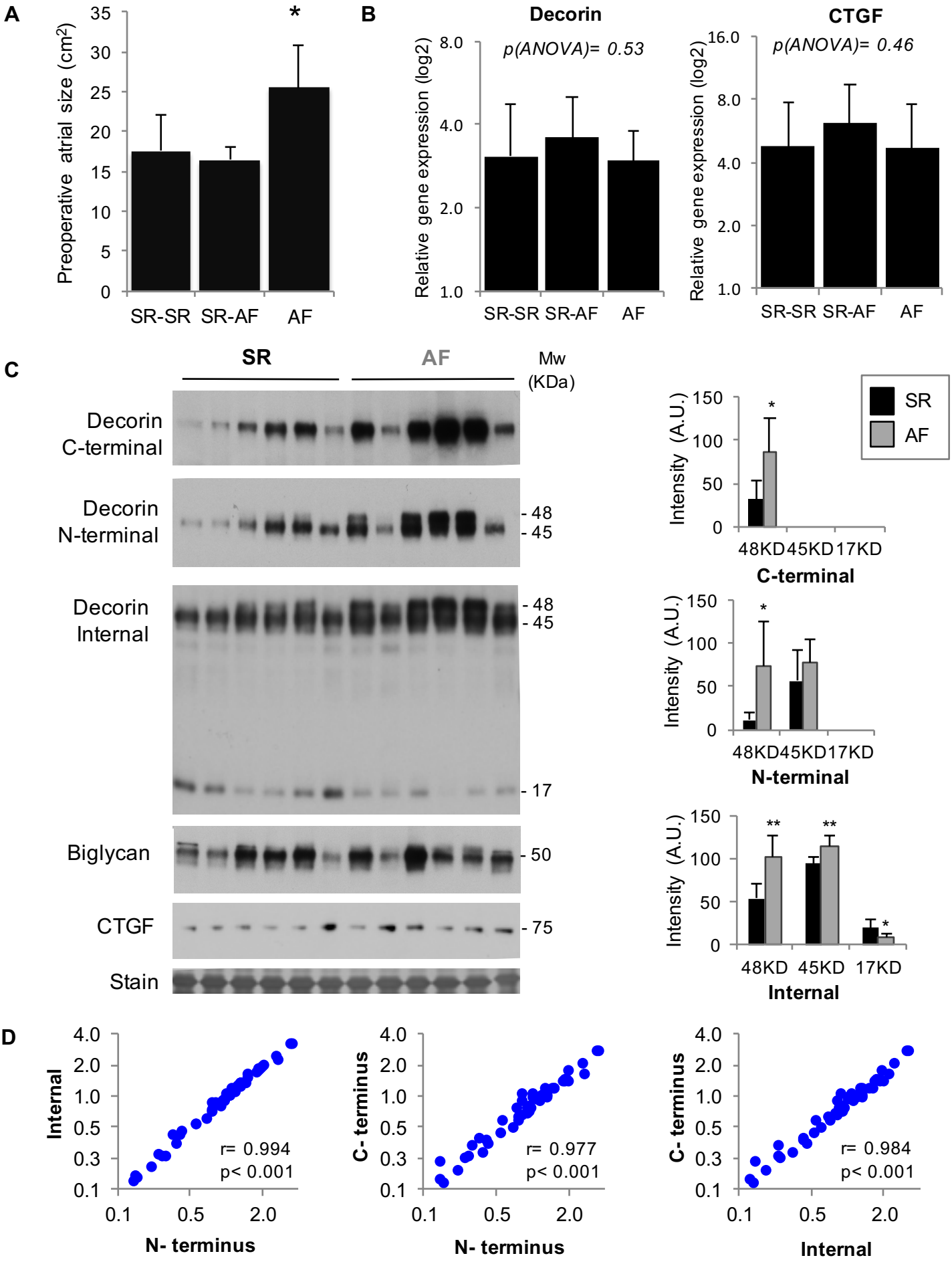

Supplementary Figure VII

A

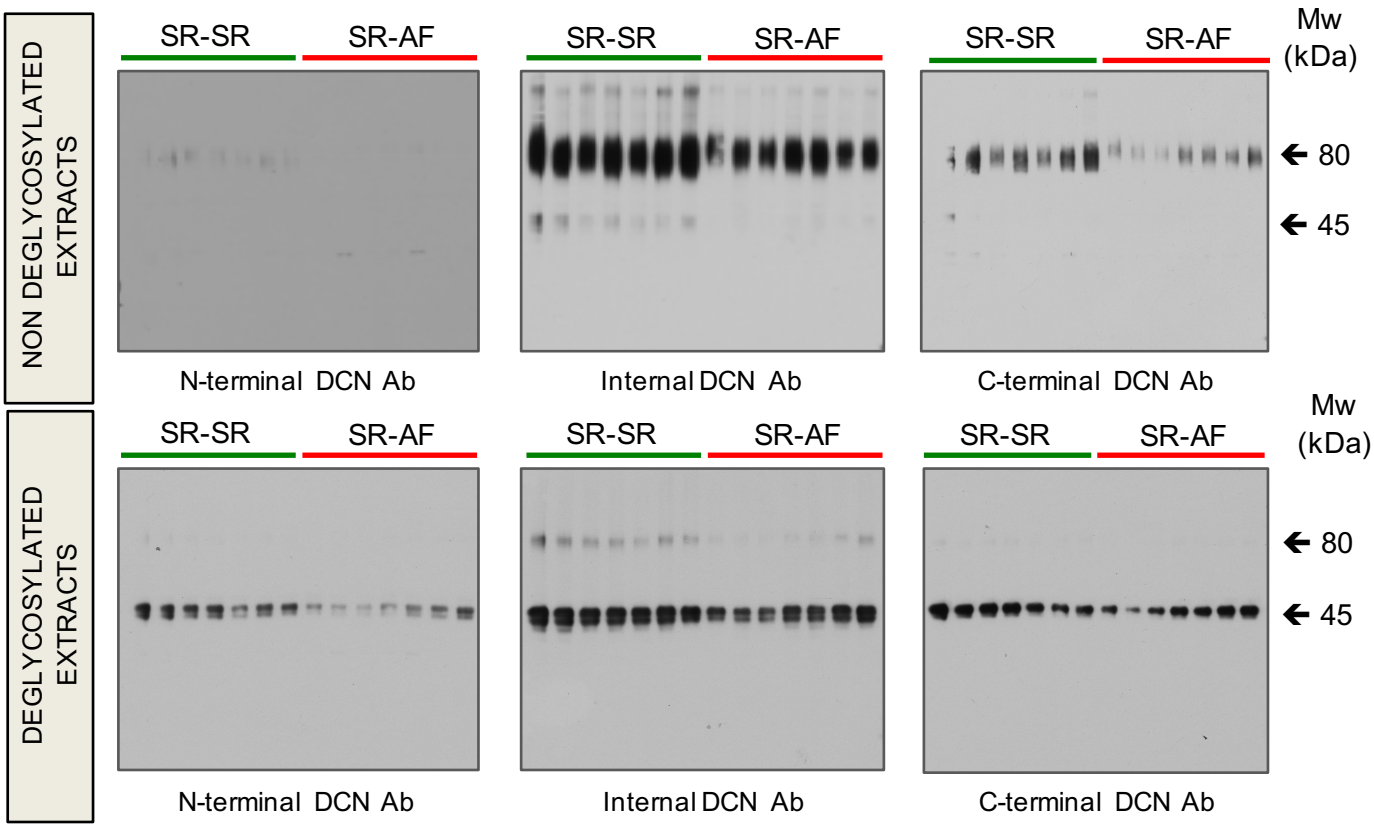

B

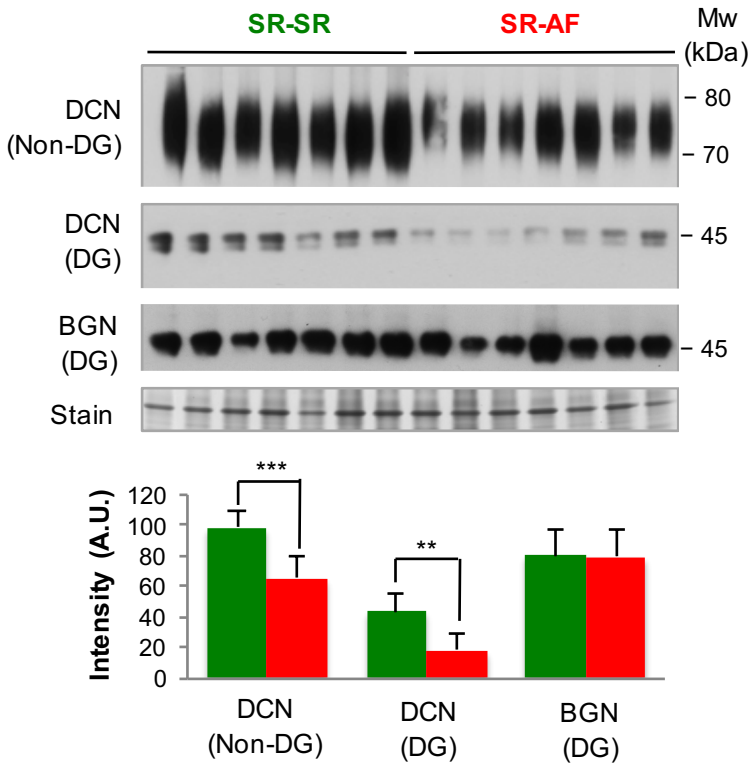

Supplementary Figure VIII

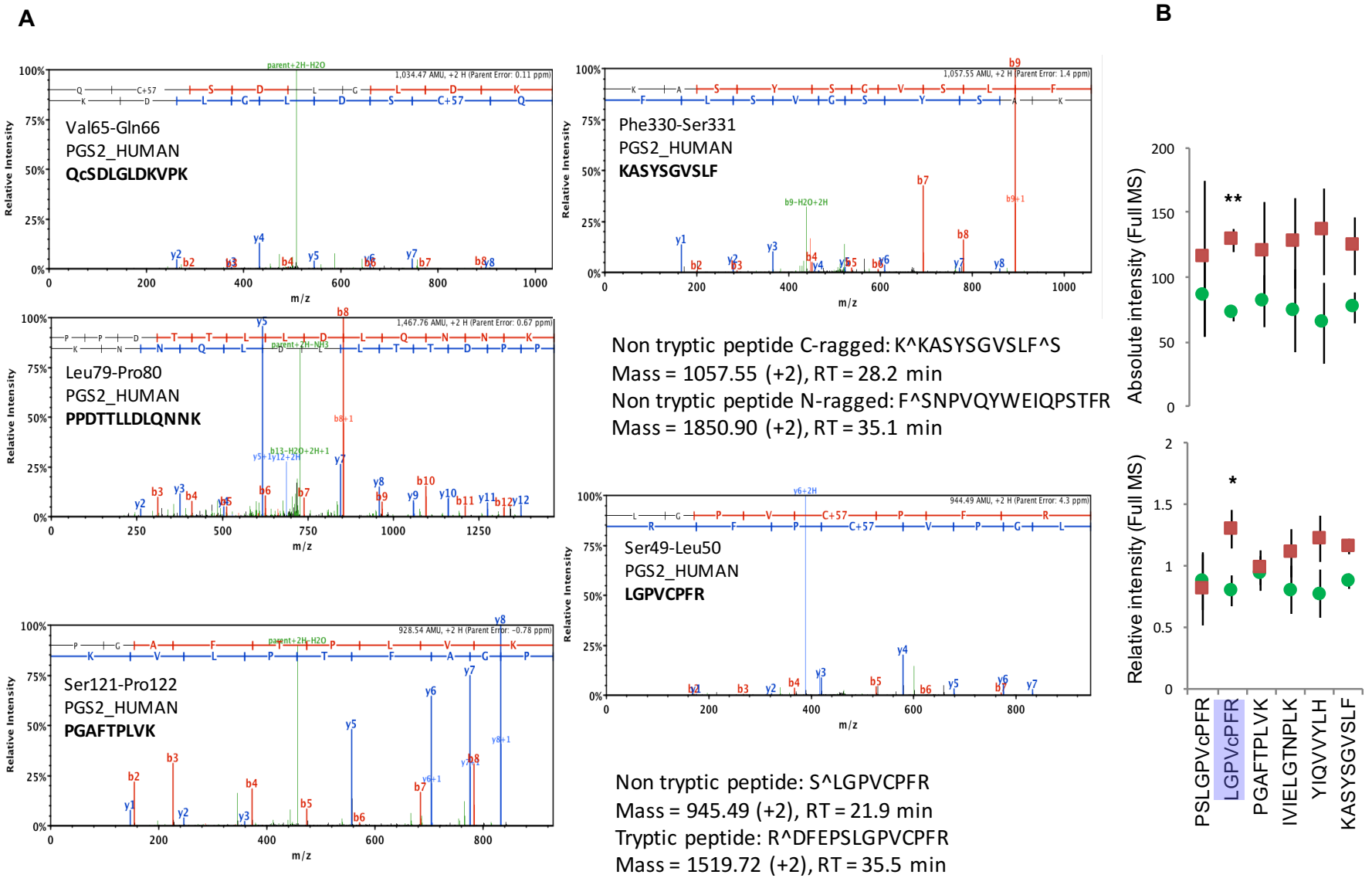

Supplementary Figure IX

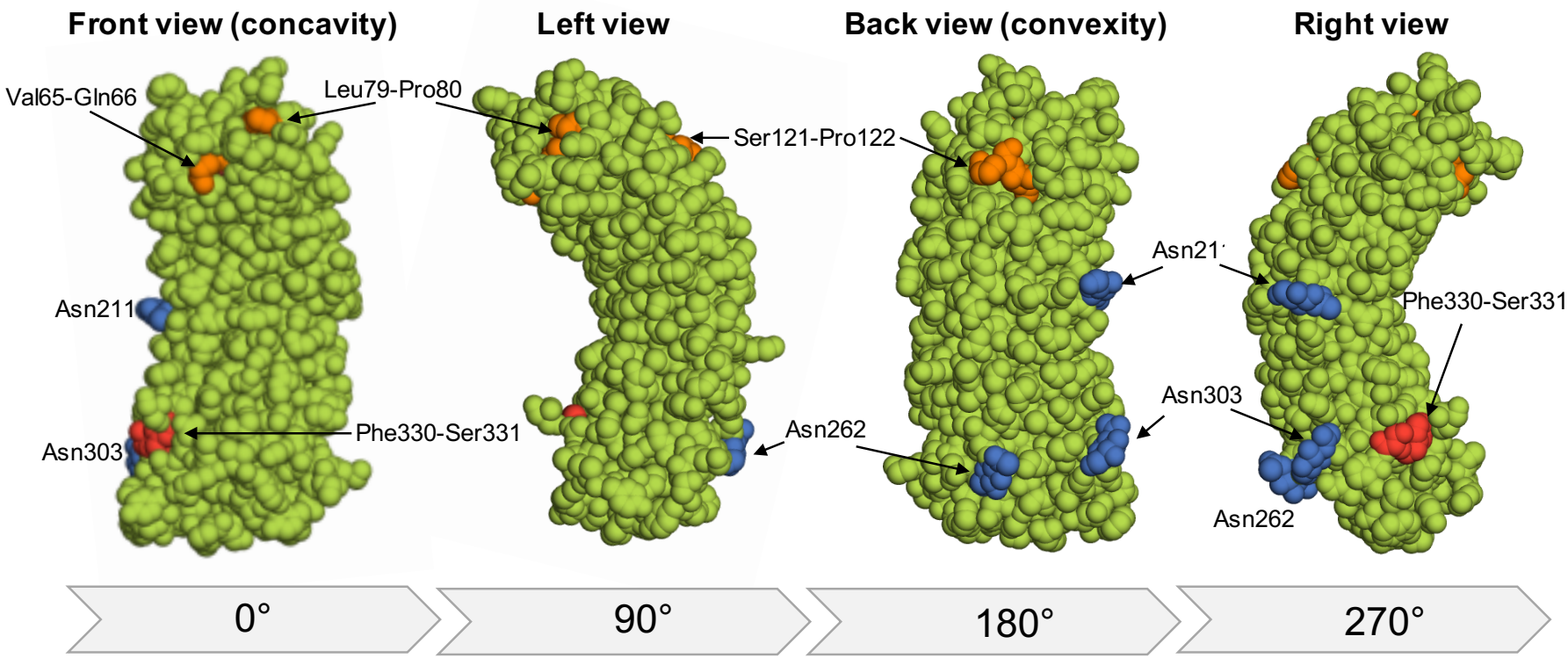

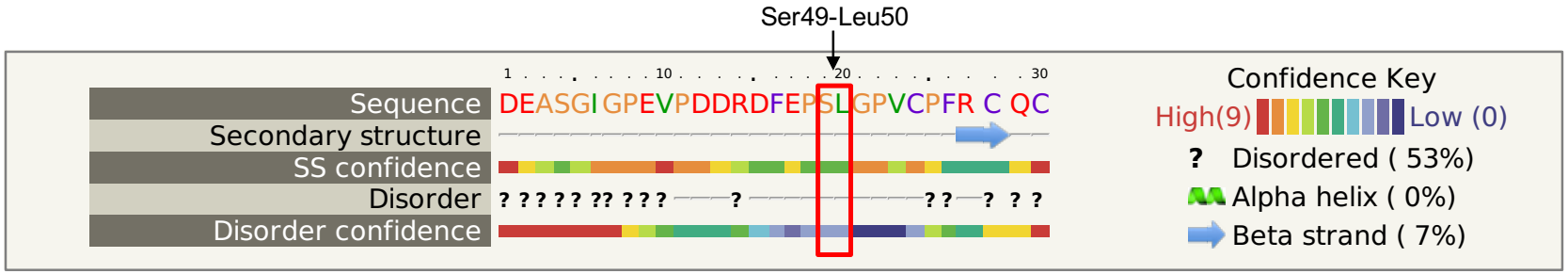

Supplementary Figure X

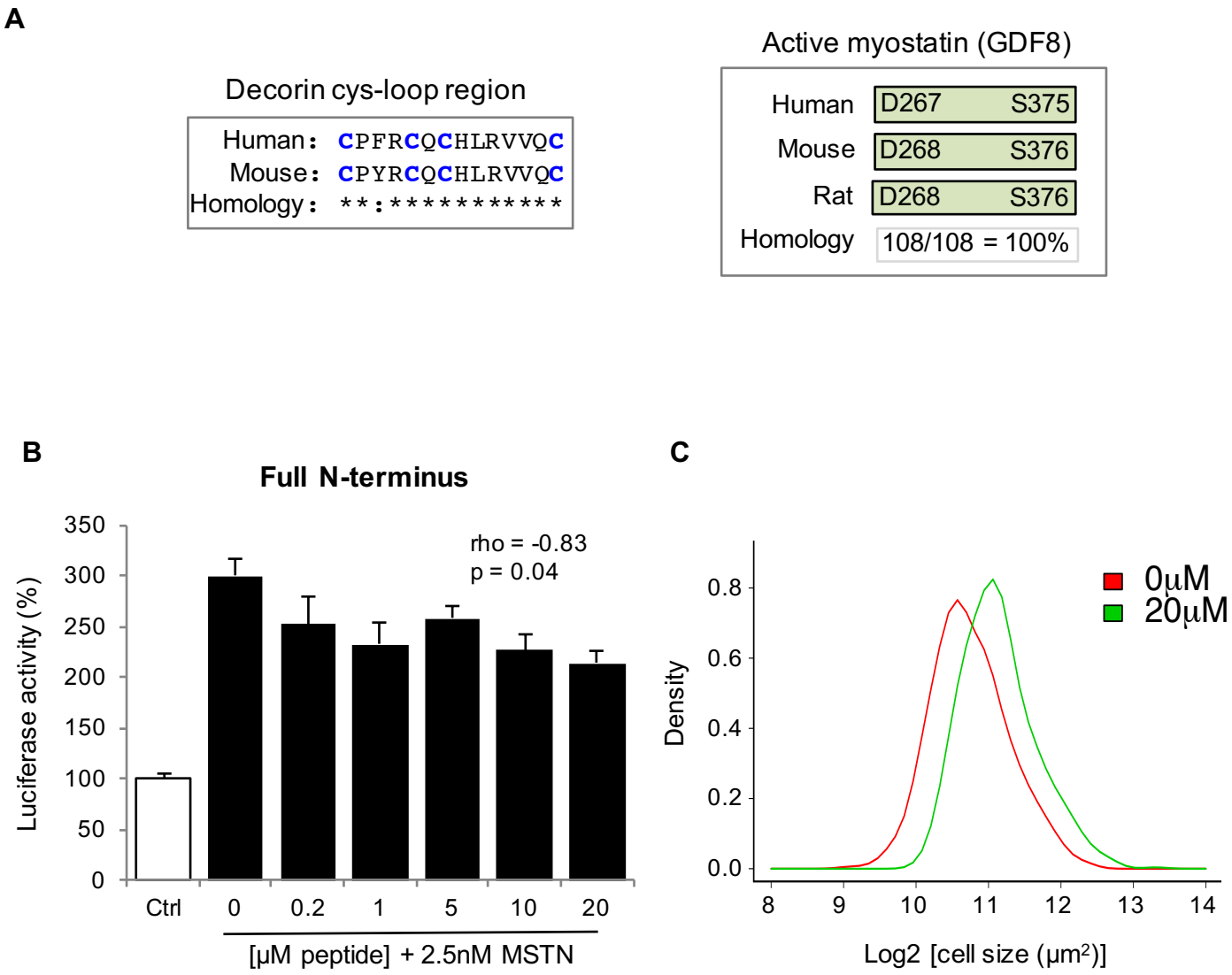

Supplementary Figure XI

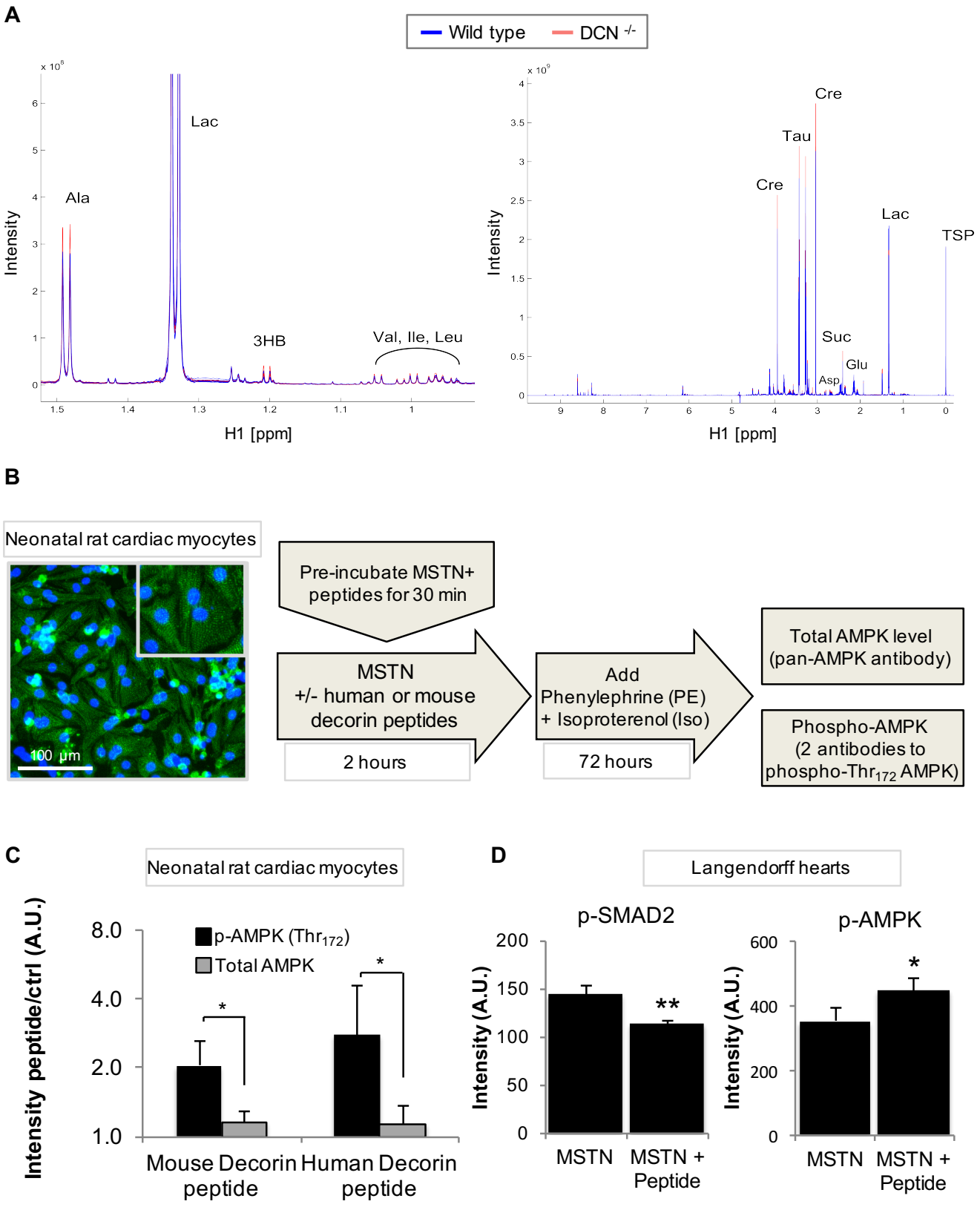

Supplementary Figure XII